Experimental evaluation of sensitivity of low-temperature combustion to intake charge temperature and fuel properties

Article *in* International Journal of Engine Research · September 2017

DOI: 10.1177/1468087417730215

CITATIONS
27

READS
1,578

2 authors:

Akhilendra Pratap Singh
Indian Institute of Technology Kanpur
102 PUBLICATIONS **3,600** CITATIONS

SEE PROFILE

Avinash Kumar Agarwal
Indian Institute of Technology Kanpur
581 PUBLICATIONS **23,176** CITATIONS

SEE PROFILE

Standard Article

International Journal of ENGINE RESEARCH

International J of Engine Research
1–26

DOI: 10.1177/1468087417730215
journals.sagepub.com/home/jer
SAGE

Experimental evaluation of sensitivity of low-temperature combustion to intake charge temperature and fuel properties

Akhilendra Pratap Singh and Avinash Kumar Agarwal

Abstract

Main challenge for mineral diesel in achieving low-temperature combustion is its poor volatility characteristics, which results in relatively inferior fuel–air mixtures. In this experimental study, feasibility of mineral diesel–fueled premixed homogeneous charge compression ignition (PHCCI) combustion was explored by employing an external charge preparation technique. An external mixing device called "fuel vaporizer" was developed for improving the fuel–air mixing. To investigate the effect of fuel properties on PHCCI combustion, this study was carried out using a variety of additives blended with mineral diesel, which included low-quality high-volatile fuel (kerosene), low-cetane high-volatile fuels (ethanol and gasoline) and high-cetane low-volatile fuel (biodiesel). To investigate the effects of intake charge temperature (T_i), experiments were performed at three T_is (160, 180 and 200 °C) and six different relative air–fuel ratios (λ = 1.5–5.25). In all experiments, exhaust gas recirculation (EGR) rate was maintained constant at 10%. Experimental results showed that combustion phasing was significantly affected by the fuel properties and T_i. At lower engine loads, volatile additives improved start of combustion, combustion phasing and heat release rate; however, excessive knocking was seen at higher engine loads. Diesoline (15% v/v gasoline with mineral diesel) and diesosene (15% v/v kerosene with mineral diesel) showed significant improvement in engine performance characteristics, while B20 (20% v/v soybean biodiesel with mineral diesel) delivered relatively higher indicated specific fuel consumption (ISFC). Increasing T_i affected fuel–air mixing, which resulted in slightly lower carbon monoxide (CO) and hydrocarbon (HC) emissions, but higher T_i led to excessive knocking and resulted in slightly higher oxides of nitrogen (NO_x) emissions. Addition of volatiles reduced particulate emissions; however, increasing T_i led to slightly higher particulate emissions. Presence of significant number of nanoparticles during combustion of B20 was another important finding of this study. Overall, it was concluded that addition of volatile additives such as gasoline, alcohols and kerosene, in addition to optimized T_i can improve mineral diesel–fueled PHCCI combustion and can lead to potentially expanded operating window.

Keywords

Partially homogeneous charge compression ignition, low-temperature combustion, fuel volatility, fuel vaporizer, heat release rate

Date received: 3 April 2017; accepted: 11 August 2017

Introduction

Harmful environmental impact of oxides of nitrogen (NO_x) and adverse health effects of particulates emitted from compression ignition (CI) engines have led to gradual evolution of stringent emission legislations for road transport sector worldwide. Exhaust from diesel engines is categorized by the World Health Organization (WHO) as "Carcinogenic." Diesel particulates are toxic because they contain traces of polycyclic aromatic hydrocarbons (PAHs). Advancements in diesel engines such as turbocharging and use of high-pressure common rail direct injection (CRDI) systems have resulted in significantly lower NO_x and particulate emissions; however, their

Engine Research Laboratory, Department of Mechanical Engineering, Indian Institute of Technology Kanpur, Kanpur, India

Corresponding author:
Avinash Kumar Agarwal, Engine Research Laboratory, Department of Mechanical Engineering, Indian Institute of Technology Kanpur, Kanpur 208016, India.
Email: akag@iitk.ac.in

levels are still higher than the limits proposed in the upcoming emissions legislations, which offer great challenge for automotive manufacturers to comply with them. Trade-off between NO_x and particulates is another major challenge for CI engines.[1] In the last few decades, low-temperature combustion (LTC) has become focus of attention for the automotive researchers. This concept has proved to be a potential alternative to conventional CI combustion due to its capability to reduce NO_x and particulate emissions simultaneously. LTC technique is based on the auto-ignition of homogeneous/premixed fuel–air mixture, without any external ignition source. Volumetric (flameless) combustion of homogeneous fuel–air mixture leads to significantly lower in-cylinder temperatures. These two factors, namely, lower in-cylinder temperatures and absence of fuel-rich zone inside the combustion chamber restrict formation of NO_x and particulates during LTC. LTC was first studied by Onishi et al.,[2] who employed this technique in a two-stroke gasoline engine to improve emission characteristics. In LTC engines, combustion is controlled by the chemical kinetics of the fuel–air mixture. To investigate detailed mechanism of LTC, Najt and Foster[3] investigated the chemical kinetics of fuel–air mixture and reported that auto-ignition of homogeneous fuel–air mixture was controlled by low-temperature chemistry (below 1000 K); however, bulk heat release during combustion was controlled by the high-temperature chemistry (above 1000 K). Due to higher volatility of gasoline, LTC techniques were easily adopted in spark ignition (SI) engines.

Improved performance and emission characteristics of LTC in SI engines motivated automotive researchers to implement these techniques in diesel engines as well. Initial research studies suggested that presence of homogeneous/premixed charge before auto-ignition was an essential requirement for LTC. However lower volatility of mineral diesel restricts its vaporization and results in charge heterogeneity inside the combustion chamber. Ryan and Callahan[4] developed port fuel injection strategy to improve the fuel–air premixing. In this methodology, mineral diesel was injected in the intake manifold, and preheated air was supplied to vaporize mineral diesel spray droplets. They reported that increasing intake air temperatures (T_i) improved the fuel–air premixing but at higher T_i, significant cool-combustion chemistry of mineral diesel resulted in rapid auto-ignition, which led to severe knocking.

For homogeneous/premixed fuel–air mixing, researchers employed in-cylinder charge preparation techniques using early direct injection (DI) and late DI.[5–9] In these techniques, fuel injection parameters, namely, start of injection (SoI) timing and fuel injection pressure (FIP), are crucial for fuel–air mixing, which directly affect the start of combustion (SoC) and heat release. However, the operating range of LTC was limited due to higher rate of pressure rise (RoPR). To resolve this issue, several researchers suggested split injection strategies.[7–9] One common conclusion emerged from these studies that lower volatility of mineral diesel increased the risk of wall wetting at advanced SoI timings.[10] Lower ignition delay of mineral diesel is another important issue related to LTC engines, which leads to knocking at higher loads.[11] To resolve these two issues, many researchers blended low cetane volatile fuel additives in order to prolong the ignition delay, which resulted in superior fuel–air mixing before the SoC, resulting in lower particulate emissions.[12,13] Chao et al.[14] carried out homogeneous charge compression ignition (HCCI) experiments using diesoline (gasoline blended with mineral diesel) and reported relatively higher thermal efficiency in HCCI combustion mode compared to SI combustion mode. They observed significant reduction in particulates emitted by diesoline, which further reduced with increasing fraction of gasoline in diesoline. Han et al.[15] carried out HCCI combustion investigations using diesoline and reported significantly lower particulate emissions due to higher volatility of diesoline. Turner et al.[16] focused on the operating window of HCCI combustion and reported that diesoline expanded the operating window of HCCI combustion by extending its lower load limit. Diesoline-fueled HCCI combustion results in superior engine stability, lower peak in-cylinder pressure and reduced hydrocarbons (HC) and carbon monoxide (CO) emissions compared to mineral diesel. Researchers also explored the potential of using diesohols (alcohol blended with mineral diesel) in CI engines and reported simultaneous reduction in particulate matter (PM) and NO_x emissions.[17–22] Ahmed[18] compared particulate emission characteristics of a heavy-duty diesel engine fueled by diesohol and baseline mineral diesel. He reported that addition of ethanol resulted in ~30–50% reduction in particulate emissions compared to mineral diesel. Ishida et al.[23] studied the combined effects of exhaust gas recirculation (EGR) and ethanol blending on HCCI combustion and reported that both EGR and ethanol addition resulted in relatively longer ignition delay. They reported that addition of ethanol significantly reduced particulate emissions due to its inherent oxygen content (34% w/w in ethanol). To explore the effect of oxygen content in test fuel, LTC investigations were conducted using biodiesel blends with mineral diesel. Fang et al.[24] performed premixed LTC experiment using biodiesel and reported slightly higher NO_x emissions due to dominance of fuel oxygen content of biodiesel over the shorter ignition delay. However, addition of biodiesel further reduced the volatility, which resulted in slightly inferior performance of LTC engines. In order to improve fuel volatility, researchers also explored the possibility of mixing kerosene with mineral diesel.[25–27] Kerosene has lower cetane number than baseline mineral diesel, which results in relatively longer ignition delay. Longer ignition delay gives a longer time for fuel–air mixing inside the combustion chamber, which leads to lower emissions. Diesosene (kerosene blended with mineral diesel) has relatively lower kinematic

viscosity and density compared to mineral diesel, which made it suitable for use in a fuel vaporizer.[28] Presence of lighter fractions of kerosene improved fuel vaporization in the vaporizer, resulting in more homogeneous fuel–air mixture formation. Engine experiments using diesosene exhibited similar combustion characteristics as that of baseline mineral diesel.[29,30] Teoh et al.[26] performed HCCI investigations by premixing kerosene in a DI diesel engine. They reported that increased fraction of kerosene in mineral diesel resulted in simultaneous reduction of HC, CO and NO_x emissions with slight increase in indicated specific fuel consumption (ISFC). However, particulate characteristics of diesosene-fueled HCCI engines have not been reported.

Many researchers used external charge preparation techniques for fuel atomization and vaporization so that homogeneous fuel–air mixtures can be prepared.[31–37] Midlam-Mohler et al.[35] and Canova et al.[36] developed a fuel atomizer for achieving mixed mode HCCI/DI combustion in a single cylinder engine. They utilized fuel atomizer to achieve HCCI combustion mode up to medium engine loads and supplied fuel by DI to achieve CI combustion mode at higher engine loads. Puschmann et al.[37] prepared homogeneous fuel–air mixture outside the combustion chamber using a "cool flame vaporizer." They used simulations to investigate the effects of intake charge temperature. Ganesh and Nagarajan[34] developed a fuel vaporizer to prepare homogeneous fuel–air mixture. The fuel vapors emitted from fuel vaporizer formed light and dispersed aerosol, which has negligible tendency of wall wetting. These tiny fuel droplets mix easily with the heated inlet air, resulting in formation of superior homogeneous charge. They did not use any external heating system to control the temperature of fuel–air mixture, which resulted in inferior performance of fuel vaporizer at higher engine loads. Midlam-Mohler[33] used a diesel atomizer to enhance the fuel atomization, which resulted in improved fuel–air mixing. They achieved HCCI combustion successfully and investigated the effect of different operating parameters on combustion. Singh and co-workers[31,32] developed a dedicated device, "fuel vaporizer," for evaporating mineral diesel–like fuels. They carried out diesel HCCI experiments to examine different control parameters and concluded that EGR was the most promising solution to optimize the combustion phasing. Other researchers also suggested that application of EGR to HCCI combustion was helpful in reducing the heat release rate (HRR) associated with intense combustion noise.[5–9,31–34] However, at lower engine loads, EGR led to inferior HCCI combustion due to significantly lower in-cylinder temperatures. Higher EGR also resulted in higher HC and CO emissions. To resolve these issues, several researchers used higher intake air/charge temperature (T_i) to improve HCCI combustion characteristics.[38–44] Singh and Agarwal[38] reported significant improvement in combustion and emission characteristics of biodiesel-fueled HCCI engine, especially at lower engine loads. Zhang et al.[39] performed HCCI experiments at higher T_i and reported significant improvement in combustion. Due to improved fuel–air mixing at higher T_i, they observed significantly lower HC and CO emissions though NO_x emissions increased slightly. Gowthaman and Sathiyagnanam[40] reported lower HC and CO emissions at higher T_i, though their study was limited up to $T_i = 60\,^{\circ}C$. Ramesh et al.[41] obtained improved brake thermal efficiency (BTE) at higher T_i. Li et al.[42] investigated the effects of T_i on the combustion characteristics of a HCCI engine fueled by n-butanol and observed stable HCCI combustion at higher T_i. Persson et al.[43] investigated the effect of varying T_i on HCCI combustion through negative valve overlap (NVO). They observed the dominant effect of T_i near the boundary of HCCI combustion operating window. At medium engine load, HCCI combustion was less affected by T_i. Asad et al.[44] explored the HCCI combustion characteristics and reported that it was predominantly chemical kinetics controlled; therefore, combustion phasing was significantly affected by T_is.

Researchers have accepted unanimously that HCCI combustion has significant potential to reduce NO_x and PM emissions. At the same time, particle number-size distribution analysis has shown some interesting facts about particulate characteristics of HCCI engines fueled using diesel-like fuels. To investigate chemical characteristics of particulates, Franklin[45] carried out HCCI experiments using mineral diesel. They reported that particulates emitted by a mineral diesel–fueled HCCI engine have relatively more volatile nucleation mode particles (NMP) compared to accumulation mode particles (AMP) and solid carbonaceous matter. Experimental studies carried out by Agarwal et al.[46,47] and Singh and Agarwal[38] showed that particulate number concentrations emitted by HCCI engine fueled by mineral diesel and B20 were significantly higher compared to gasoline-fueled SI engine. This was mainly due to significantly higher volatility of gasoline compared to diesel-like fuels. To investigate the effects of fuel volatility on particulate characteristics, Bergstrand[30] carried out experiments using diesosene and mineral diesel, and reported lower particulate emissions from diesosene at lower engine loads; however, he did not reported anything about particulate composition. Few studies on HCCI engine particulate characteristics also reported significant contribution of nanoparticles (NPs) in the HCCI exhaust.[38,48] These particles are difficult to intercept by the exhaust gas aftertreatment devices. Kittelson[49] concluded that reduction in particulate mass from HCCI engine resulted in higher NPs, leading to higher toxicity. Fialkov[50] proposed that NPs were formed mainly due to copious ions and electrons generated during fuel oxidation up to $\sim\#10^{10}$–$10^{11}/cm^3$ and showed a correlation with HCCI combustion since it was pre dominantly controlled by chemical kinetics of the fuel–air mixture.

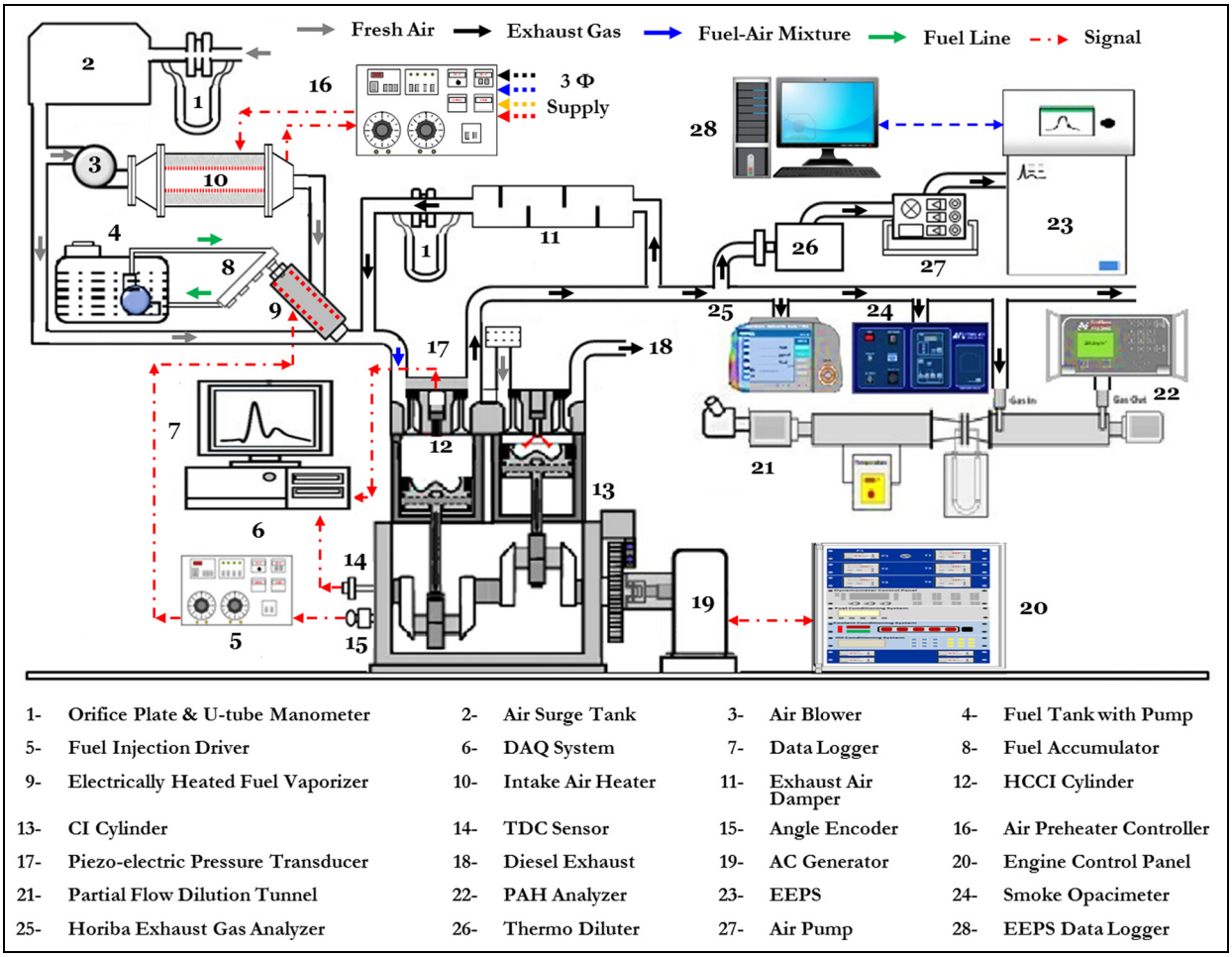

Figure 1. Schematic of the experimental setup for PHCCI investigations.

The literature shows significant potential of LTC for low-quality volatile fuels; however, shortcomings of these studies were not investigated in subsequent studies. Previous studies showed that variation in Ti and fuel volatility affected LTC significantly, and performance of LTC engine fueled by low-quality volatile fuels can be improved by varying these parameters. Above-mentioned studies were focused on some specific aspects of LTC. Combined investigation of these two parameters on LTC engines fueled by low-quality volatile additives has not been carried out. These two parameters together affected fuel–air mixing mainly under extreme load conditions and directly influenced the operating range of LTC engines. Therefore, this study is aimed at investigating premixed homogeneous charge compression ignition (PHCCI) engine combustion, performance, emissions and particulate characteristics using different test fuels, namely, B20, diesoline (15% gasoline with mineral diesel), diesohol (15% ethanol with mineral diesel) and diesosene (15% kerosene with mineral diesel) vis-à-vis baseline mineral diesel. Experiments were performed at three different T_i's (160°, 180° and 200° C) and six engine loads. For premixed/homogeneous fuel–air mixing, an external fuel–air mixing device "fuel vaporizer" was used. Temperature of the charge produced by this vaporizer was controlled by an intake air heating system such that the performance of the vaporizer was not adversely affected by engine load and fuel properties.[27] Use of low-quality high-octane fuels in advanced combustion techniques is the innovative aspect of this study. Detailed particulate characterization including particulate number-size distribution and trace metal concentration determination are some other important areas, which have not been discussed in previous studies.

Experimental setup and methodology

In this study, a constant speed, two-cylinder, four-stroke air-cooled DI diesel engine (DA16; Kirloskar) was used for PHCCI investigations. For loading the engine, a single phase 11-kW, 220-V alternating current (AC) generator was coupled to the test engine. This engine–generator system was connected to a 10-kW resistive load bank. Schematic of the experimental setup is shown in Figure 1.

For PHCCI combustion investigations, one cylinder of the engine was modified to operate in PHCCI combustion mode. The second cylinder of the engine was operated in conventional CI combustion mode, which

Table 1. Specifications of the test engine used for PHCCI combustion experiments.

Engine characteristics	Specifications	
	Unmodified CI cylinder	Modified PHCCI cylinder
Make/model	Kirloskar/DA16	ERL-3/IIT Kanpur
Fuel injection type	Direct injection	Port injection
Fuel injection timing	24° bTDC	45° bTDC
Fuel injection release pressure	210 bar at 1500 r/min	3 bar at 1500 r/min
Compression ratio	17.5:1	16.5:1
Power output/cylinder	5.5 kW at 1500 r/min	4.15 kW at 1500 r/min
Displacement per cylinder	779 cc	779 cc
Bore/stroke	95/110 mm	
Cooling system	Air-cooled	

CI: compression ignition; PHCCI: premixed homogeneous charge compression ignition; bTDC: before top dead center.

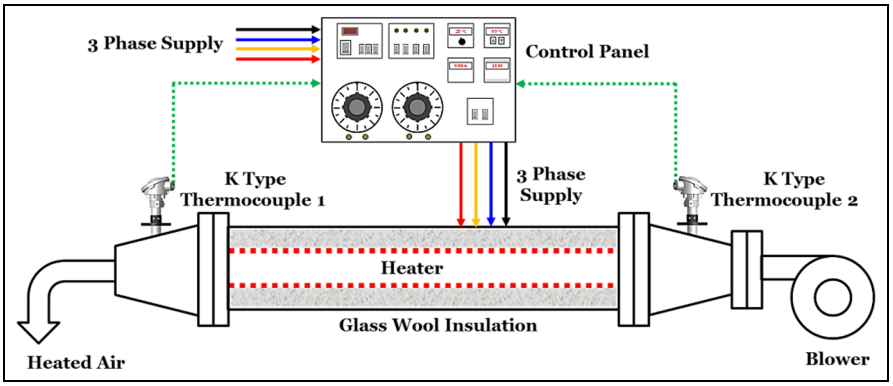

Figure 2. Schematic of the intake air heating system and its controller.

acted as a power plant to start the PHCCI engine. Both cylinders of the engine were modified according to the experimental requirements. To reduce knocking during PHCCI experiments, compression ratio of the PHCCI cylinder was reduced from 17.5 to 16.5. For collecting the exhaust gas samples for emission characterization, exhaust manifold of the PHCCI mode cylinder was separated from the CI mode cylinder. For controlling the HRR in the PHCCI cylinder, a fraction of exhaust gas was recirculated to the intake manifold of the PHCCI cylinder. Specifications of the test engine and important modifications are given in Table 1.

For controlling the T_i, an air heating system was installed in the experimental setup. This intake air heating system consisted of an electric heater (12 kW), heater controller, one air blower and several thermocouples for measuring temperature. The intake air heating system was installed downstream of the inlet surge tank. Schematic of the intake air heating system and its controller is shown in Figure 2.

To measure the volumetric air flow rate, an orifice plate and a U-tube manometer were used upstream of the surge tank. A blower was placed in between the surge tank and the air preheater to supply high-velocity intake air (blast air) into the fuel vaporizer. For controlling the temperature of the blast air, a closed-loop proportional–integral–derivative (PID) controller was used, which precisely controlled the temperature up to ±3 °C. The heater controller took feedback from a thermocouple installed upstream of the preheater.

In the PHCCI cylinder, fuel was supplied via the fuel vaporizer. Fuel injection system of CI mode cylinder was not changed; however, for the PHCCI mode cylinder, a low-pressure fuel injection system was used. This fuel injection system consisted of a fuel injector, fuel accumulator, electric drive low-pressure fuel pump (Denso; 1500M844M1), fuel tank and injector driver circuit. Electrical drive low-pressure fuel pump supplied the test fuel to the fuel accumulator, which in turn delivered high-pressure fuel to the port fuel injector. This injector operated on a 12-V TTL (transistor–transistor logic) pulse given by the injector driver circuit. Injector driver circuit took input of top dead center (TDC) signal and triggered the timing integrated circuit (IC555) for generating TTL output pulse. For cycle reference signal (TDC signal), an inductive proximity sensor (GLP18APS; Transducers and Allied Products) was installed on the engine camshaft.

Lower volatility of mineral diesel was one of the prime concerns in achieving LTC for diesel-like fuels. Therefore, development of an external fuel–air mixing device, known as “fuel vaporizer” is the main achievement of this study. This fuel vaporizer can easily convert

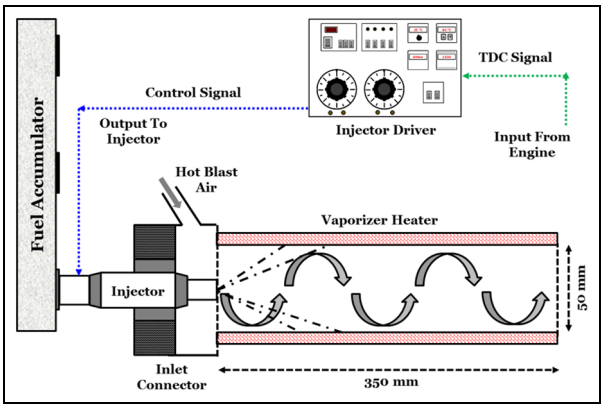

Figure 3. Schematic of the fuel vaporizer.

liquid fuel droplets from diesel spray into the vapor form. Schematic of the fuel vaporizer is shown in Figure 3. Fuel vaporizer has three sections namely, main vaporizing chamber, inlet connector with provision for blast air, and an electric heater. Main vaporizing chamber was made of aluminum, which was covered externally by a ceramic band heater. To improve the fuel–air mixing inside the main vaporizing chamber, a probe was connected to the vaporizer for supplying preheated air at very high velocity. The angle of this probe was adjusted to improve air motion inside the chamber.

To control the warm-up time and cut-off temperature of the heater, an electric heater was connected to a voltage regulator. Temperature of the fuel vaporizer was controlled by the PID controller, which was connected to a thermocouple installed at the outlet connector of the fuel vaporizer. Important specifications of the fuel vaporizer are given in Table 2.

In the fuel vaporizer, a port fuel injector was used to inject liquid fuel into the preheated main vaporizer chamber. When fuel spray strikes the chamber walls, small fuel droplets absorb thermal energy from the heated walls and vaporize. Fuel vapors provided by this device form light-dispersed aerosol, which follows the air motion. High-velocity intake air supplied by the air preheater forces these fuel vapors to mix with the intake air to form a partially homogeneous fuel–air mixture. This mixture was then supplied to the combustion chamber through the intake valve. Temperature of this homogeneous mixture was considered as the T_i for PHCCI combustion mode.

For combustion analysis, an online data acquisition system (DAQ) was installed. This DAQ system includes piezoelectric pressure transducer (6013C; Kistler), precision optical angle encoder (365C; AVL) and compact combustion measurement system (IndiMicro; AVL) with data acquisition software (IndiCom Mobile; AVL). Optical angle encoder was used for angle-related measurement, which acted as an interface between the engine crank angle position and the DAQ clock pulse. Combustion measurement system converts the voltage signal of the piezoelectric pressure transducer into the in-cylinder pressure data. Data acquisition software calculates different combustion parameters such as RoPR, HRR, SoC, combustion phasing and combustion noise.

Table 2. Specifications of the fuel vaporizer.

Characteristics	Specifications
Power supply to the heater	2.0 kW
Main vaporizer chamber diameter	50 mm
Length of vaporizer	350 mm
Warm-up time	3 min

For the measurement of regulated emissions from the PHCCI cylinder, an exhaust gas emission analyzer (MEXA584L; Horiba) was used, which measured raw concentrations of gaseous species namely, NO_x, HC, CO and carbon dioxide (CO_2). For particulate characterization, an engine exhaust particle sizer™ (EEPS 3090; TSI) was used. EEPS is capable of measuring particles in the size range from 5.6 to 560 nm. It can measure maximum particle concentration up to 10^8 particles/cm^3 of the exhaust gas. For measurement of PAH concentration in the exhaust gas, an online PAH analyzer (PAS 2000; EcoChem Labs) was used. This analyzer was capable of real-time measurement of particulate bound PAHs in ng/m^3. For particulate composition analysis, a partial flow dilution tunnel was used to collect the particulates emitted by the engine on a preconditioned filter paper. Particulates sampling duration and dilution ratio were kept constant (30 min and 13.5, respectively) for all test fuels. Particulate-laden filters were analyzed for trace metals using inductively coupled plasma–optical emission spectrophotometer (ICP-OES) (iCAP DUO 6300 ICP Spectrophotometer; Thermo Fischer Scientific).

In this study, different test fuels, namely, B20, diesoline, diesohol and diesosene vis-à-vis baseline mineral diesel were used to investigate PHCCI combustion. These test fuels were selected on the basis of their properties such as calorific value, viscosity, density and fuel volatility. Diesoline and diesosene showed almost similar calorific values while diesohol had ~10% lower calorific value compared to baseline mineral diesel. Densities of all test fuels were almost similar though B20 showed highest density amongst all test fuels. Important properties of these test fuels are given in Table 3.

Comparison of volatility of these test fuels showed that the distillation curve of B20 was above the baseline mineral diesel, while those of diesoline, diesohol and diesosene were below (Figure 4). Among all test fuels, B20 exhibited the lowest volatility, while diesoline displayed the highest volatility. Distillation curves of diesoline, diesohol and diesosene also reflected that the volatility of mineral diesel improved by addition of highly volatile fuel additives such as gasoline, ethanol and kerosene. Furthermore, the distillation curves of

Table 3. Test fuel properties.

Property	Mineral diesel	B20	Diesoline	Diesohol	Diesosene
Blend composition	100% mineral diesel	20% biodiesel and 80% mineral diesel	15% gasoline and 85% mineral diesel	15% ethanol and 85% mineral diesel	15% kerosene and 85% mineral diesel
Calorific value (MJ/kg)	43.54	42.63	43.79	39.67	43.72
Density (g/cc) at 30 °C	0.831	0.846	0.807	0.814	0.827
Viscosity (cSt) at 40 °C	2.82	3.17	2.69	2.78	2.64
Flash point (°C) (min)	~54	~71	–	~46	~50

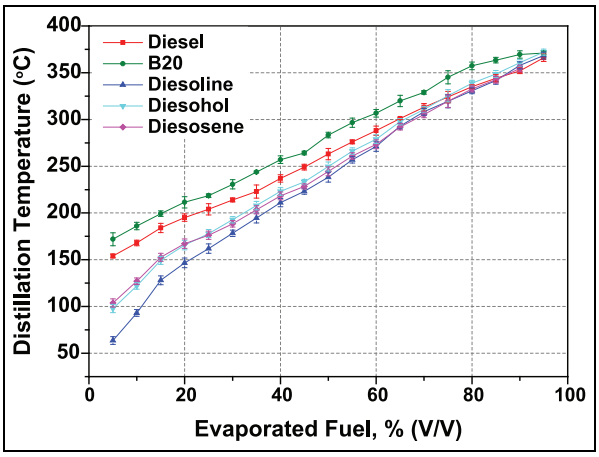

Figure 4. Fuel distillation characteristics.

these test fuels showed larger differences at lower distillation temperatures, which narrowed with increasing distillation temperatures. At high-distillation temperatures, effect of volatile additives became less significant.

Results and discussion

In this study, PHCCI combustion was investigated for different test fuels, namely, B20, diesoline, diesohol and diesosene vis-à-vis baseline mineral diesel. PHCCI combustion mode experiments were performed at constant EGR (10%), three different T_is (160, 180 and 200 °C) and six different engine loads. Experimental matrix is shown in Table 4.

Objective of these experiments was to select suitable T_i for PHCCI combustion fueled by different test fuels having different fuel properties. This section is divided into five sub-sections, namely, combustion, performance, emissions, particulates, and trace metal emission characteristics of the PHCCI engine fueled by the different test fuels.

Combustion analysis

The combustion behavior of the test fuels in PHCCI mode were evaluated in detail through monitoring and analysis of different parameters. Figure 5 shows the variation of in-cylinder pressure w.r.t. crank angle as a function of fuel–air ratios (λ) and test fuels. In this figure, before top dead center (bTDC) position is

Table 4. Experimental matrix.

	Test fuels: mineral diesel, B20, diesoline, diesohol and diesosene; EGR = 10%		
Load ↓	T_i = 160 °C	T_i = 180 °C	T_i = 200 °C
λ = 5.25	√	√	√
λ = 4.50	√	√	√
λ = 3.75	√	√	√
λ = 3.00	√	√	√
λ = 2.25	√	√	√
λ = 1.50	√	√	√

represented by negative crank angle degree (CAD) and after top dead center (aTDC) position by positive CAD. This P–θ diagram provides in-depth information of other relevant combustion parameters including SoC, combustion phasing, end of combustion (EoC), RoPR and HRR. Comparison of in-cylinder pressure curves and motoring curve clearly showed auto-ignition of these test fuels at all loads. Slope of in-cylinder pressure curves is a measure of RoPR, which is directly governed by chemical kinetics of the charge. SoC for all test fuels showed a shift towards bTDC in case of richer fuel–air mixtures (Figure 5(a), (d), (g), (j), (m) and (p)). This was due to presence of large fuel quantities in the combustion chamber, which promoted rapid auto-ignition of the fuel–air mixtures.

At higher engine loads ($\lambda < 3$), all test fuels displayed significantly advanced SoC (~15–20 CAD bTDC) (Figure 5(a), (e) and (h)), but at lower loads, mineral diesel and B20 showed relatively retarded SoC (Figure 5(l), (o) and (r)). Lower volatility of mineral diesel and B20 was the reason for this behavior. Among more volatile test fuels (diesoline, diesohol and diesosene), slightly retarded SoC of diesohol was because of its higher auto-ignition temperature and poor miscibility of ethanol with mineral diesel. At lower engine loads, effect of volatile additives such as gasoline, kerosene and ethanol can be observed, which improves PHCCI combustion.

At higher T_i (T_i = 200 °C), addition of these volatile additives was less prominent than at lower T_i (T_i = 160 °C). This was attributed to faster chemical kinetics of fuel–air mixtures, which dominated over fuel volatility. However, at lower engine loads, combination of both (1) improved fuel volatility and (2) faster

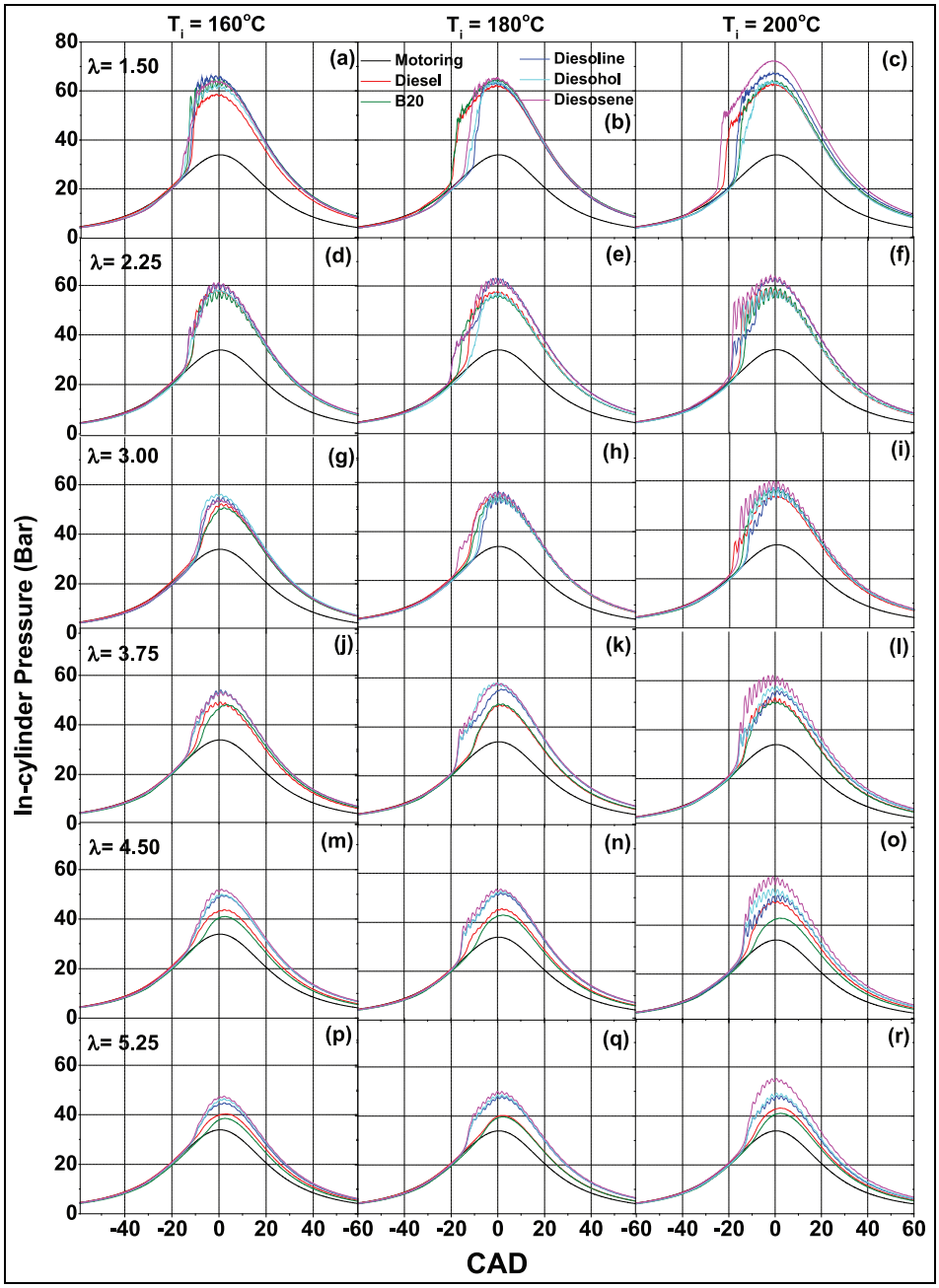

Figure 5. (a-r) Variation of in-cylinder pressure of the PHCCI engine fueled by mineral diesel, B20, diesoline, diesohol and diesosene at varying loads and T_i.

chemical kinetics of fuel–air mixtures improved PHCCI combustion. Knocking was observed for all test fuels, when fuel–air mixtures were relatively richer ($\lambda < 3.75$). Highest knock tendency was displayed by diesoline and diesosene because of their lower cetane numbers and auto-ignition temperatures.

Overall, the knocking tendency of test fuels was higher at $\lambda = 2.25$ in comparison to other loads (Figure 5(d)–(f)). PHCCI combustion at $\lambda = 1.5$ caused knocking spread over longer crank angles with an average of 250 cycles showing diminishing knock behavior (Figure 5(a)–(c)).

In-cylinder pressure curves also showed that diesosene exhibited the highest maximum pressure (P_{max}) amongst test fuels (Figure 5(c), (f), (i), (l), (o) and (r)). This was due to relatively higher calorific value and lower cetane number of diesosene, which resulted in higher ignition delay and led to relatively longer premixed combustion compared to higher cetane number test fuels.[30] For all test fuels, P_{max} decreased with increasing λ because of lower injected fuel quantity. At higher engine loads (lower λ), P_{max} of mineral diesel and B20 were comparable to that of other test fuels, however at lower engine loads, mineral diesel and B20

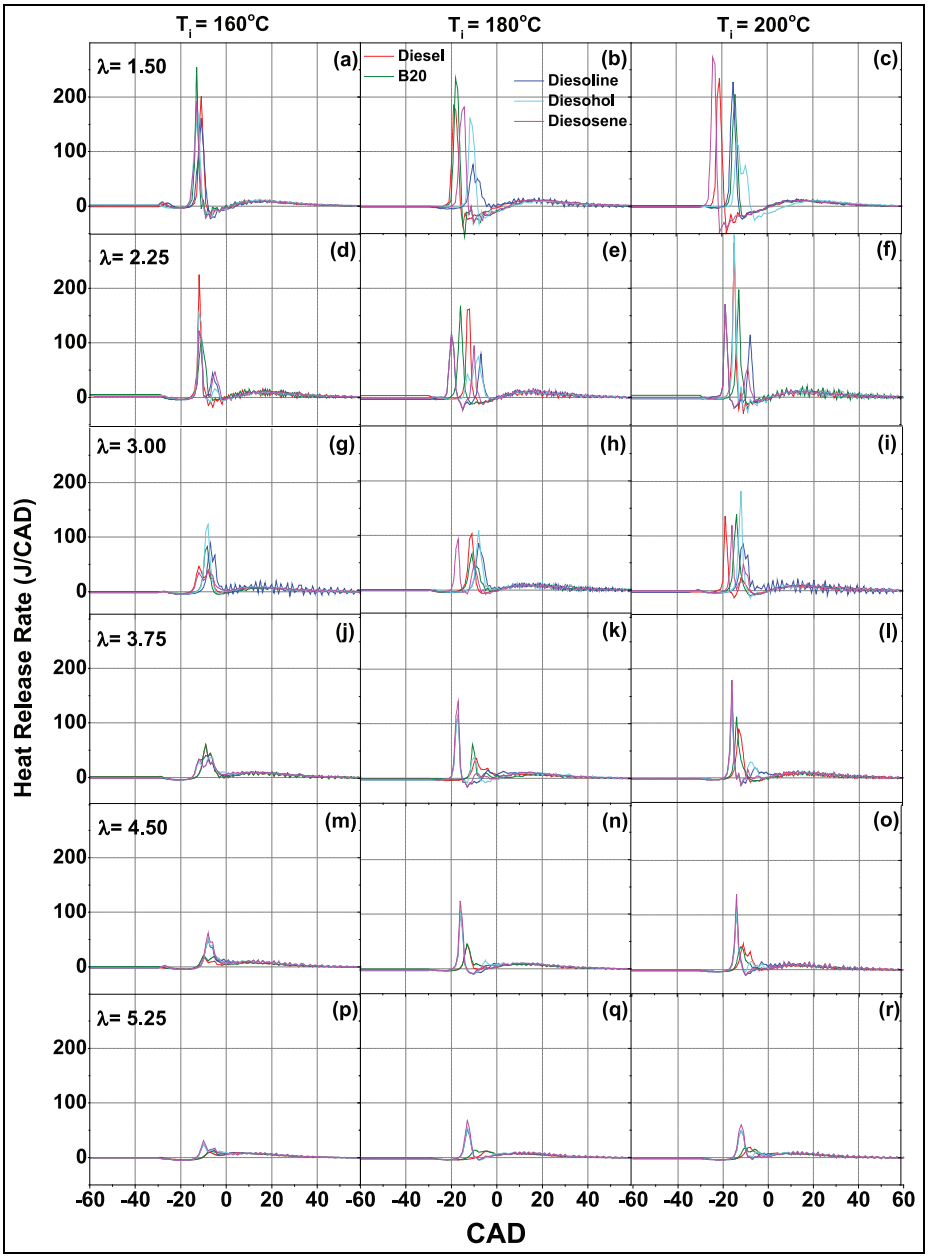

Figure 6. (a-r) Heat release rate of the PHCCI engine fueled by mineral diesel, B20, diesoline, diesohol and diesosene at different loads and T_is.

showed significantly lower P_{max} compared to diesoline, diesohol and diesosene. The position of P_{max} was another important parameter, which provided qualitative information of combustion phasing in PHCCI combustion. Earlier P_{max} positions were observed for richer fuel–air mixtures of diesoline and diesosene. These differences however reduced with increasing λ (Figure 5(a)–(g)). Main reason for variation of P_{max} position at lower loads was the presence of volatile fuel components (gasoline, ethanol and kerosene) in lower quantities in the baseline mineral diesel. From the slopes of in-cylinder pressure curves (Figure 5(a)–(r)), it was observed that RoPR increased with increasing engine load (i.e. decreasing λ) and T_i.

HRR analysis (Figure 6) is an important parameter for characterizing PHCCI combustion. HRR patterns of PHCCI combustion of diesoline, diesohol and diesosene were different than that of baseline mineral diesel and B20. At higher engine loads (richer fuel–air mixtures), PHCCI combustion showed significantly higher HRR compared to conventional CI combustion. Higher HRR for richer mixtures was because of presence of higher fuel quantity, which enhanced fuel–air mixture reactivity and kinetics.

Advanced SoC due to faster fuel–air mixture chemical kinetics was also observed from the HRR curves (Figure 6(a)–(g)). At most engine loads, diesosene showed maximum HRR followed by diesoline. The two most important properties responsible for this trend were the higher calorific values and lower cetane numbers of kerosene and gasoline. Lower boiling

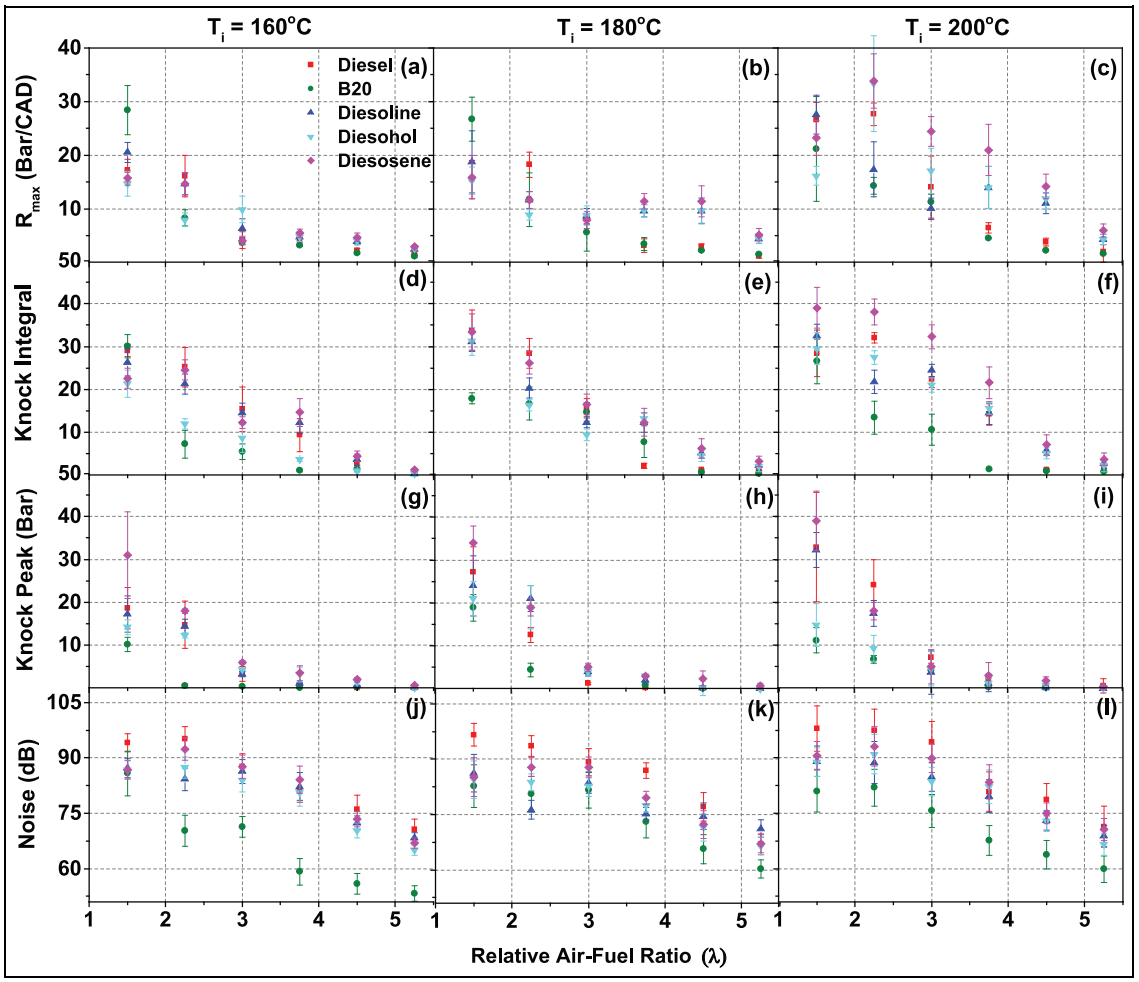

Figure 7. (a-c) Maximum pressure rise rate, (d-f) knock integral, (g-i) knock peak and (j-l) combustion noise of the PHCCI engine fueled by mineral diesel, B20, diesoline, diesohol and diesosene at varying loads and T_is.

temperature/range of gasoline and kerosene were also responsible for this behavior, which enhanced fuel volatility and improved mixture homogeneity. HRR increased with increasing T_i, and the effect was more prominent at lower engine loads. With increasing λ, HRR of the test fuels decreased drastically due to reduction of fuel quantity in the combustion chamber and slower combustion kinetics. At lower engine loads, mineral diesel and B20 showed significantly lower HRR compared to other test fuels. Therefore, effect of volatile additives can be clearly seen at lower engine loads (Figure 6(o)–(r)).

Figure 7 shows the maximum pressure rise rate (R_{max}), knock integral (KI), knock peak (KP) and combustion noise in the PHCCI engine at different engine loads and T_is. KI represented the integral of superimposed rectified knock oscillations, and KP reflected the absolute maxima of the rectified knock oscillations superimposed on the cylinder pressure curve. Knocking parameters were determined from the pressure signals, which were filtered through a high-pass filter and then rectified. Parameters such as KI or KP of the superimposed oscillations were determined from the measured signals. Noise level was calculated from the cylinder pressure signals.[51] Knocking during PHCCI combustion occurred essentially because of the ignition delay that caused a late pressure wave inside the combustion chamber and generated noise. Noise and knock parameters were controlled by HRR, which were affected by the cetane number, fuel quantity injected and combustion efficiency of the test fuels. When the fuel quantity injected increased, R_{max} during PHCCI combustion also increased (Figure 7(a)–(c)). This resulted in unacceptable noise (Figure 7(j)–(l)) (due to severity of detonation). This phenomenon can potentially damage the engine and lead to unacceptably high NO_x levels. During PHCCI combustion at lower loads (lower fuel quantity injected), RoPR decreased and combustion phasing retarded, leading to decreased in-cylinder pressures and temperatures, which ultimately resulted in lower noise.

Figure 7 shows that R_{max} of the test fuels reduced with increasing λ. R_{max} was also affected by the fuel–air mixture reactivity, which increased with increasing T_i. At T_i = 200 °C, R_{max} reached up to 30 bar/CAD; therefore experiments were limited up to λ = 1.5

(Figure 7(c)). Maximum R_{max} was observed for diesoline and diesosene, whereas B20 showed minimum R_{max}. This clearly showed the effect of cetane number of test fuels, since fuels having lower cetane number resulted in higher R_{max}. At lower T_i, diesoline showed maximum R_{max} (Figure 7(a)), and as T_i increased, diesosene and mineral diesel dominated over diesoline (Figure 7(b) and (c)). At lower T_is, higher fuel volatility of diesoline and diesosene dominated, but at higher T_i, relatively lower volatility of mineral diesel was compensated by higher T_i, which resulted in faster fuel–air mixture reaction kinetics and led to higher R_{max} (Figure 7(c)). These results showed an important observation that the operating range of PHCCI combustion could be extended by selecting suitable fuel composition and control parameters.

KI was used to analyze the knocking behavior of PHCCI combustion. At lower loads, KI was lower and it increased with increasing engine load. This was due to enrichment of fuel–air mixtures with increasing engine load, which led to higher mixture reactivity. At $\lambda = 1.5$, KI was the maximum due to excessive knocking (Figure 7(d)–(f)). These results were similar to in-cylinder pressure results (Figure 5). KI was the maximum for mineral diesel (at lower T_i) and diesosene (at higher T_i) due to the higher cetane number of kerosene (~35) and superior combustion efficiency, respectively. Figure 7(g)–(i) shows KP for each test fuel. KP mainly depends on HRR of PHCCI combustion. Diesosene showed higher HRR (Figure 6), which resulted in higher KP compared to other test fuels. At higher T_i, diesoline showed slightly higher KP compared to diesosene (Figure 7(i)). At most T_is and load conditions, B20 resulted in minimum KP. This was mainly due to higher cetane number and lower reactivity of biodiesel, which further resulted in slower fuel–air mixture kinetics compared to other test fuels. Combustion noise was also affected by HRR. Noise levels were less than 90 dB at lower loads, but for relatively richer fuel–air mixtures, noise levels were in the range considered dangerous for human exposure. Maximum noise level measured was ~105 dB for mineral diesel (Figure 7(l)). Diesoline and diesohol had lower cetane numbers, which caused relatively lower combustion noise. For diesohol, combustion efficiency was controlled primarily by the moisture content and was responsible for medium KI and noise level. B20 showed minimum combustion noise amongst all test fuels. This was mainly due to its higher viscosity, which resulted in retarded SoC with combustion shifting towards diffusion combustion phase.

Figure 8 shows the effect of different volatile additives on timings of various combustion events such as SoC, combustion phasing and combustion duration (CD) at varying engine loads and T_is. From Figure 8(a)–(c), it can be observed that SoC retarded for the test fuels as the fuel–air mixtures became leaner. This mainly resulted because of slower fuel-air chemical kinetics under lean conditions; therefore, it took longer time to start the combustion thus retarding the SoC timings. SoC of diesosene was relatively earlier compared to mineral diesel, B20, diesoline and diesohol. Relatively higher cetane number (compared to gasoline and ethanol) and lower auto-ignition temperature (compared to mineral diesel and biodiesel) of kerosene were the reasons for this behavior. Diesohol and B20 showed retarded SoC compared to other test fuels. Presence of moisture traces in diesohol reduced the mixture reactivity, hence retarded the SoC. Furthermore, ethanol was unlikely to auto-ignite under standard CI conditions because of its lower octane number. This was another important reason for retarded SoC of diesohol compared to other test fuels. For B20, higher viscosity and poor volatility were important factors behind retarded SoC. SoC advanced with increasing T_i, and this trend was common for all test fuels (Figure 8(a)–(c)). This was due to relatively faster fuel–air kinetics at higher T_i.

Figure 8(d)–(f) showed the variation in combustion phasing (CA_{50}) for all test fuels at different engine loads and T_i's. PHCCI combustion is significantly affected by combustion phasing, which reduced for very advanced combustion phasing as well as for very late combustion phasing. Optimum combustion phasing was found at medium engine loads ($\lambda = 3.0$–4.5) and intermediate T_i (Figure 8(e)). All other combustion parameters investigated also revalidated this λ range and T_i as optimized PHCCI combustion conditions. Diesoline showed superior combustion phasing compared to mineral diesel, B20, diesohol and diesosene. At higher loads, combustion phasing for diesosene advanced though B20 and diesohol showed retarded combustion phasing (Figure 8(e) and (f)). At lower loads, retarded combustion phasing of mineral diesel and B20 resulted in poor combustion efficiencies, which was also observed from the in-cylinder pressure curves (Figure 5).

Figure 8(g)–(i) show the variation of CD at different engine loads and T_is. CD affected both engine performance as well as emissions. In PHCCI mode, CD was affected by SoC because too advanced SoC resulted in shorter CD, whereas retarded SoC showed slightly longer CD. Too short CD resulted in higher R_{max}, which led to inferior engine performance due to knocking. However, too long CD resulted in relatively lower engine power output. Shorter CD was typically observed in the PHCCI engine due to volumetric combustion of charge in the combustion chamber. Relatively longer CD was observed at $\lambda = 4.5$ and 5.25, which led to lower peak in-cylinder temperatures. CD was also affected by the fuel quantity injected and fuel–air mixture reactivity. At $\lambda = 3.75$–1.5, CD decreased due to extremely high mixture reactivity, leading to very fast combustion (Figure 8(h) and (i)), which bordered knocking combustion. Figure 8 shows that CD of mineral diesel and B20 were relatively longer compared to other test fuels. Lower fuel–air mixture reactivity of these test fuels was the prime reason for this trend. Relatively lower volatility of mineral

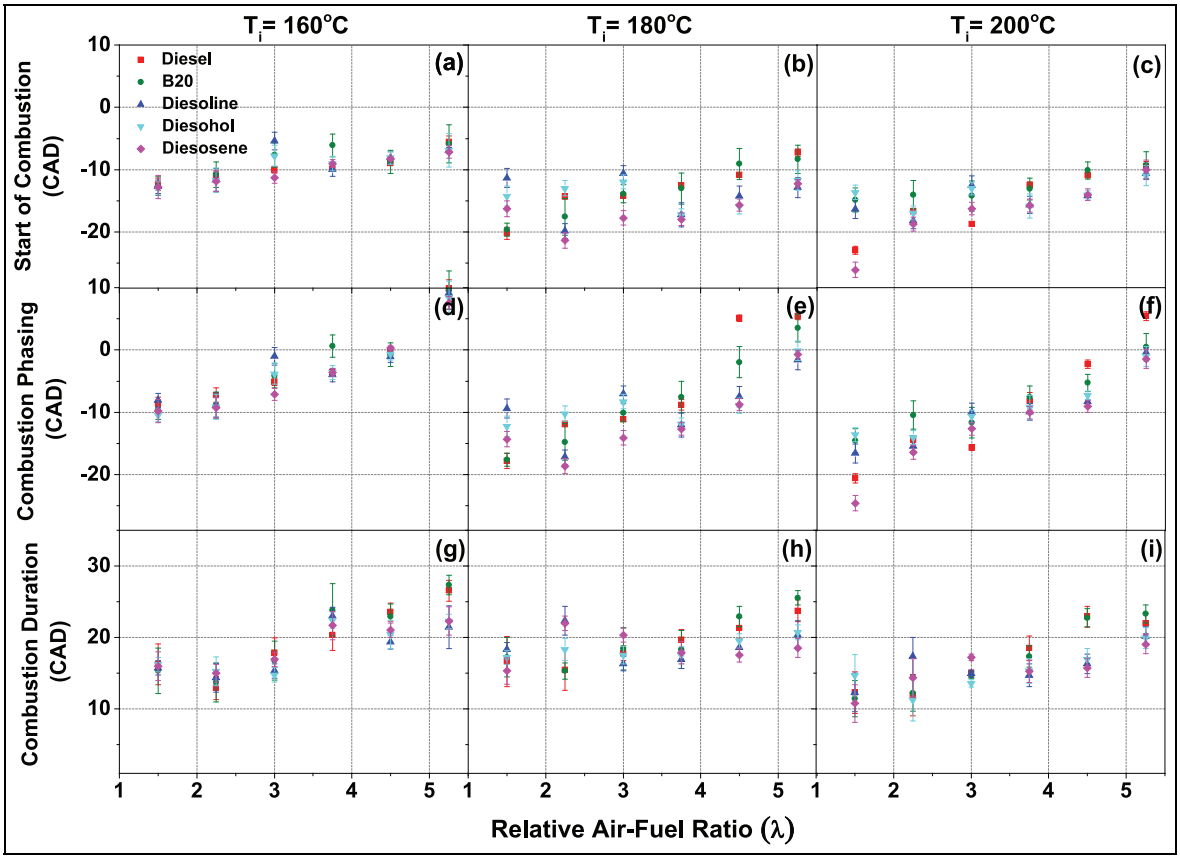

Figure 8. (a-c) Start of combustion, (d-f) combustion phasing and (g-i) combustion duration in the PHCCI engine fueled by mineral diesel, B20, diesoline, diesohol and diesosene at varying loads and T_is.

diesel and biodiesel was another important reason for this behavior, which significantly reduced fuel–air mixing compared to other more volatile test fuels. Combustion phasing was another factor, which affected CD. As the combustion phasing retarded (mineral diesel and B20), CD became relatively longer (Figure 8(e) and (h)) since the maximum cycle temperature decreased. However, at higher engine loads, mineral diesel resulted in shorter CD. Presence of larger fuel quantity in the combustion chamber at the time of ignition was the main reason for this behavior.

Performance characteristics

In the engine experiments, indicated thermal efficiency (ITE), ISFC, indicated specific energy consumption (ISEC), exhaust gas temperature (EGT) and indicated mean effective pressure (IMEP) were analyzed as the main performance parameters. EGT was measured separately for both cylinders, i.e. CI combustion mode cylinder and the PHCCI combustion mode cylinder.

Figure 9(a)–(c) showed the variations of ITE for all test fuels at different engine loads and T_is. At medium engine loads (λ = 3–3.75), PHCCI combustion resulted in almost comparable ITE as that of conventional CI combustion. Relatively lower heat losses compared to conventional CI or SI engines due to lower peak combustion temperatures and shorter CD were the main reasons for higher ITE in PHCCI combustion mode. In addition, PHCCI engine utilized homogeneous charge, which did not generate soot during combustion; therefore, radiative losses were almost nonexistent. Relatively lower heat losses compensated for lower in-cylinder temperatures, resulting in higher ITE. For all test fuels, ITE increased with increasing engine load (up to medium loads, λ = 3.75) due to presence of richer fuel–air mixtures. However, at higher engine loads, ITE decreased due to relatively earlier SoC (Figure 8(a)–(c)), which led to higher heat losses from the cylinder walls and piston; hence, lower work was done on the piston by the expanding gases, resulting in reduced engine efficiency. At lower T_i (Figure 9(a)), diesoline and diesosene showed the maximum ITE amongst all test fuels. With increasing T_i, ITE of mineral diesel improved slightly at higher engine loads; however at lower engine loads, diesosene and diesoline displayed relatively higher ITE.

This showed importance of addition of volatile additives in mineral diesel. At all T_is and engine loads, B20 showed the lowest ITE. Combustion phasing was an important factor for this behavior. At higher engine loads, diesosene and diesoline showed slightly advanced combustion phasing, but at all loads, B20 showed retarded combustion phasing. Both conditions

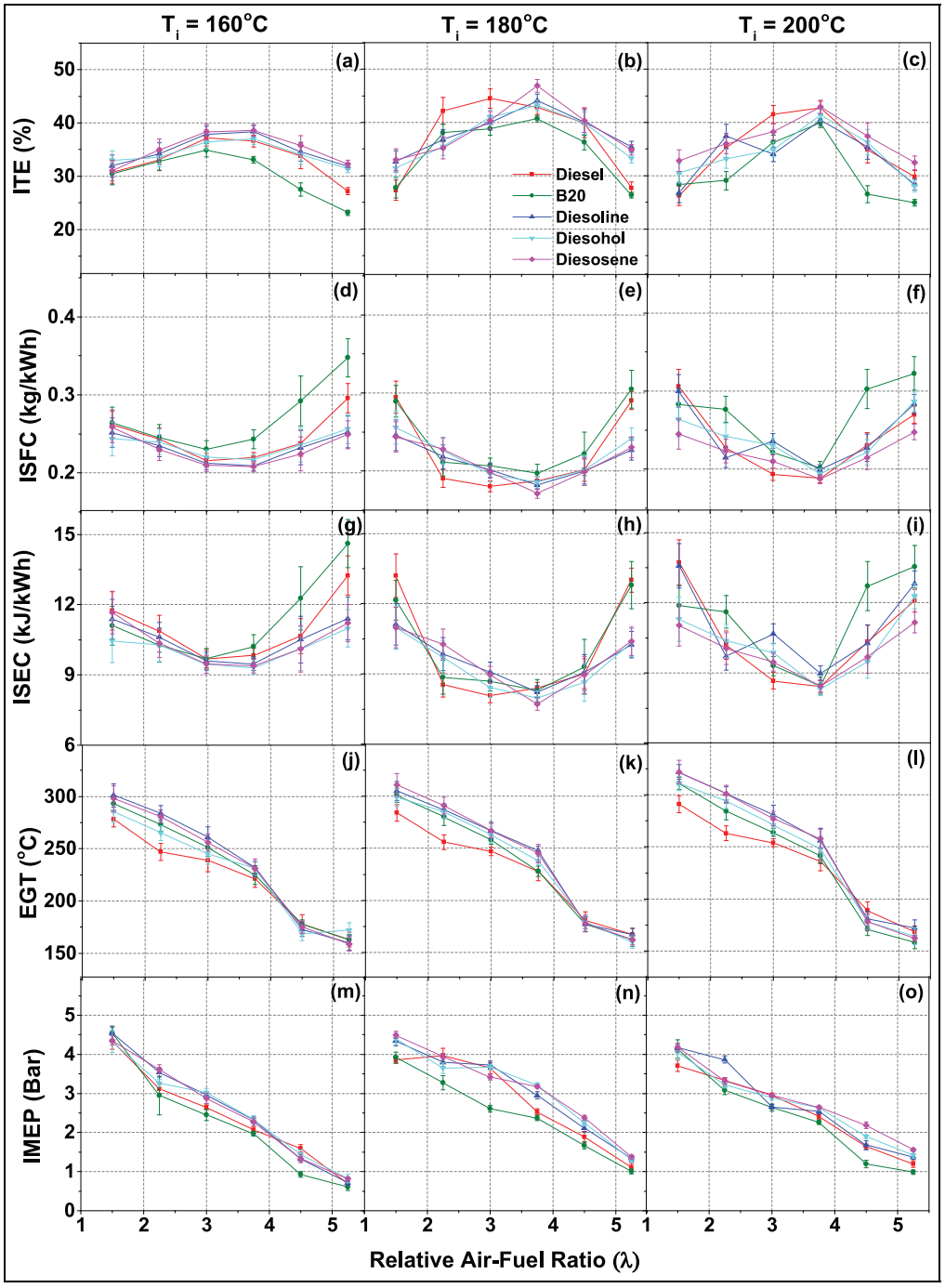

Figure 9. (a-c) ITE, (d-f) ISFC, (g-i) ISEC, (j-l) EGT and (m-o) IMEP of the PHCCI engine fueled by mineral diesel, B20, diesoline, diesohol and diesosene at different engine loads and T_is.

adversely affected combustion efficiencies and resulted in lower ITE. At lower engine loads, mineral diesel and B20 showed sharp reduction in ITE due to dominating effect of lower fuel volatility, which affected chemical reactions in fuel–air mixture. Increasing T_i (up to $T_i = 180\,^{\circ}C$) improved PHCCI combustion due to faster fuel–air chemical kinetics and resulted in relatively higher ITE for all test fuels (Figure 9(e)). However, at very high T_i (200 °C), excessive knocking in PHCCI combustion resulted in relatively lower ITE (Figure 9(f)). Figure 9(d)–(f) showed that all test fuels had nearly similar ISFC at higher engine loads; however, at lower engine loads, mineral diesel and B20 showed slightly higher ISFC compared to other test fuels. Relatively lower ITE in case of mineral diesel and B20 was the reason for this trend. Among all test fuels, diesoline showed abnormal performance at intermediate loads ($\lambda = 3.0$). This was also observed in the combustion characteristics (Figures 5(i) and 6(i)). At intermediate loads, diesoline showed significantly retarded combustion compared to other engine operating conditions. A relative dominance of lower cetane number

over T_i at intermediate engine load might be a possible reason for this abnormal trend. For all test fuels, minimum ISFC was observed at medium loads. Main reason for this trend was relatively higher increase in power output compared to increase in fuel consumption. ISEC (Figure 9(g)–(i)) for different test fuels was calculated, and the trend was found similar to that of ISFC. ISFC and ISEC reduced with increasing T_i; however, at higher T_i (200 °C), ISFC and ISEC increased due to relatively lower power output. Figure 9(j)–(l) showed that PHCCI combustion resulted in significantly lower EGT compared to conventional CI combustion, and this was the main reason for ultra-low NO_x emissions from the PHCCI engine. Diesoline and diesosene showed slightly higher EGT compared to other test fuels due to relatively higher calorific values and improved volatility of these test fuels. Both these factors improved PHCCI combustion and resulted in higher in-cylinder temperatures, which led to higher EGT. Diesohol showed slightly lower EGT compared to diesoline and diesosene. Moisture traces in the fuel affected the reaction rates, which led to slightly inferior combustion efficiencies and resulted in slightly lower EGT. Among all test fuels, mineral diesel showed slightly lower EGT, and the EGT of B20 was relatively higher. Presence of oxygen in B20 was the main reason for this trend, which improved combustion. At lower loads, EGT for all test fuels was almost equal because of lower reactivity of leaner fuel–air mixtures and lower fuel quantities. For all test fuels, EGT increased with increasing T_i; however, the differences were not significant. Figure 9(m)–(o) showed the variation of net IMEP for the test fuels at different engine loads and T_is. Net IMEP, the main performance parameter, was affected by combustion characteristics such as combustion phasing and CD. Figure 9(m)–(o) showed that diesosene and diesoline exhibited the highest net IMEP, followed by diesohol. At higher engine loads, diesosene, diesoline and diesohol showed comparable net IMEP. Among all test fuels, B20 showed the lowest net IMEP. All test fuels showed slight reduction in net IMEP. This was due to occurrence of knocking at higher T_i, which was relatively more dominant in case of diesosene and mineral diesel.

Emission characteristics

Figure 10 shows the emission characteristics (CO, HC CO_2 and NO_x) and PAHs emissions from the PHCCI engine fueled by different test fuels. Figure 10(a)–(c) showed that all test fuels followed similar trend of CO emissions, which increased with increasing λ. CO emissions were mainly due to incomplete combustion of fuels in PHCCI combustion mode. PHCCI combustion showed slightly higher CO emissions compared to conventional CI combustion mode. At lower engine loads, presence of leaner fuel–air mixtures resulted in relatively lower in-cylinder temperatures, which prevented oxidation of CO into CO_2. At higher loads, ISCO emission was almost similar for all test fuels; however, diesohol showed relatively lower ISCO at lower engine loads.

Among all test fuels, B20 and mineral diesel showed relatively higher CO emission at lower engine loads. Inferior combustion due to lower volatility of these fuels was the main reason for this behavior. For all test fuels, CO emission decreased with increasing T_i. At higher T_i, superior conversion of CO into CO_2 was the main factor responsible for reduction in CO emission. At higher T_i, mineral diesel and other relatively more volatile test fuels showed significant difference in CO emission compared to that at lower T_i. However, CO emission from B20 were affected to a lesser degree by higher T_is. This was due to lower fuel volatility and higher viscosity of B20, which dominated the increased T_i.

Figure 10(d)–(f) showed the variation in HC emissions at different engine loads and T_is. HC emissions in PHCCI combustion mode were generally higher than conventional CI combustion mode. Relatively lower in-cylinder temperatures were the main reason for higher HC emissions. Although for leaner fuel–air mixtures, lower peak in-cylinder temperature in PHCCI mode reduced NO_x formation; however these low temperatures also resulted in higher HC emissions. Combustion temperatures near the cylinder walls further lowered due to heat losses. Combustion quenching in the vicinity of cylinder walls also resulted in higher HC emissions. Figure 10(d)–(f) showed that HC emissions slightly increased with increasing λ. Retarded combustion phasing at lower engine loads was the main reason of this behavior. With increasing engine load, all test fuels showed nearly constant HC emissions. This was due to two mutually opposing effects. On increasing the engine load, combustion chamber temperature increased, which resulted in lower HC emissions; however, at higher engine loads, slightly inferior performance of fuel vaporizer resulted in slightly higher HC emissions. At higher engine loads, some liquid fuel droplets entered engine cylinder and moved into the crevice volume. During expansion stroke, they emerged out into the combustion chamber along with crevice gas and contributed towards overall HC emissions. This was another reason for higher HC emissions from low-volatility fuels such as mineral diesel and B20 in the PHCCI engine (Figure 10(d)–(f)). Increasing T_i reduced HC emissions from mineral diesel and B20. This was due to improved fuel vaporization at higher T_is. With increasing T_i, HC emissions from volatile test fuels were not affected significantly. At T_i = 180 °C, HC emissions slightly reduced (Figure 10(e)) because of improved combustion; however, at T_i = 200 °C, HC emissions further increased (Figure 10(f)) due to in-cylinder knocking. CO_2 emission is an indirect measure of combustion efficiency. Higher CO_2 emissions show efficient combustion. In the PHCCI engine, CO_2 emissions were affected by both, test fuel quantity (engine load) and test fuel properties. With increasing engine load, CO_2 emissions from PHCCI engine increased due to presence of higher fuel quantity (Figure 10(g)–(i)). With increasing T_i, CO_2 emissions increased due to improved combustion and superior

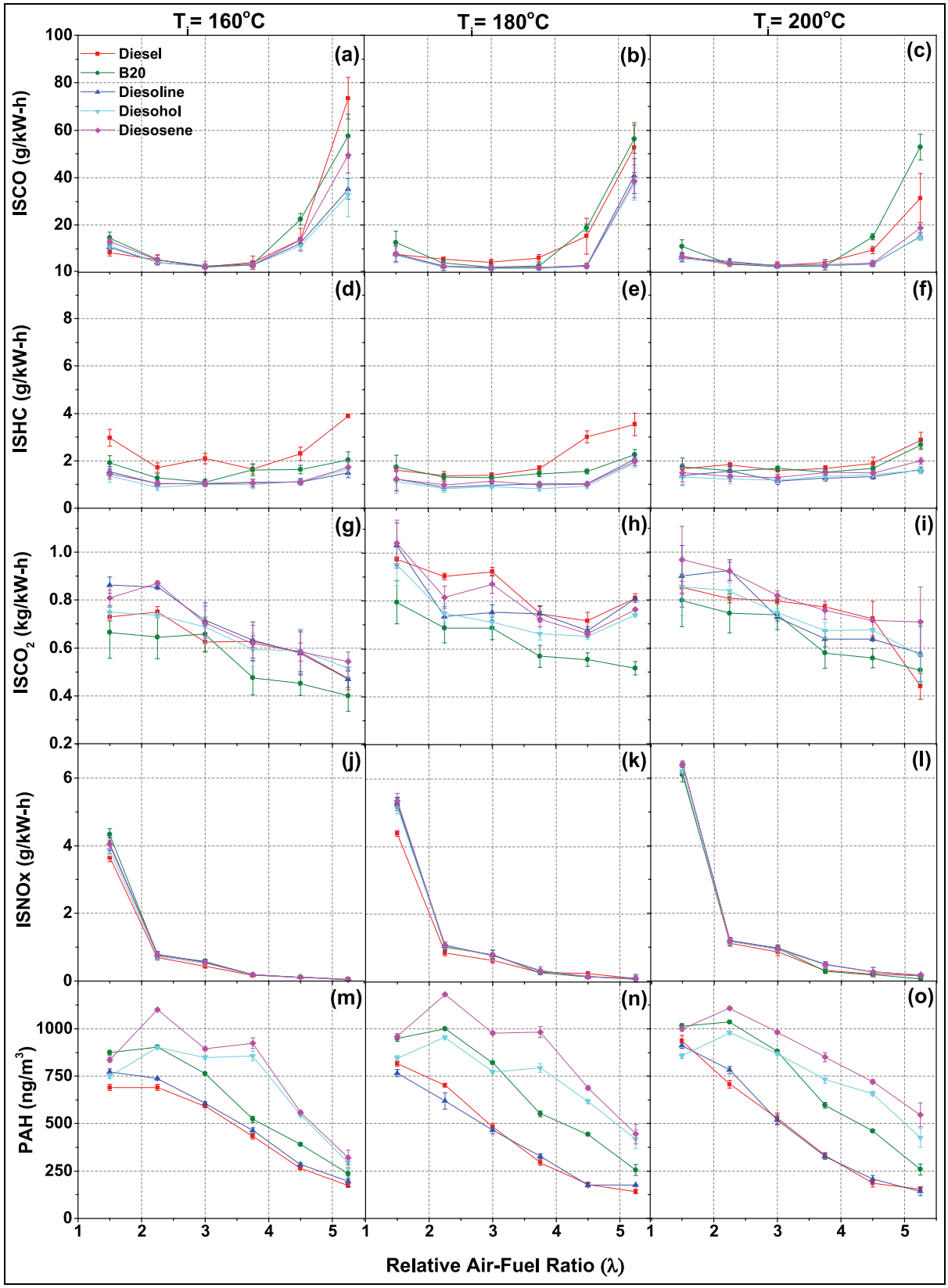

Figure 10. (a-c) ISCO, (d-f) ISHC, (g-i) $ISCO_2$, (j-l) $ISNO_x$ and (m-o) PAHs emissions from the PHCCI engine fueled by mineral diesel, B20, diesoline, diesohol and diesosene at different engine loads and T_is.

conversion of CO into CO_2. Comparison of CO_2 emission behavior of different test fuels showed higher CO_2 emissions from mineral diesel and diesosene. Among all test conditions, B20 showed the lowest CO_2 emissions. Variations in CO_2 emission was also affected by the engine performance.

Ultra-low NO_x emission is the main advantage of PHCCI combustion. NO_x formation is sensitive to peak combustion chamber temperature. Figure 10(j)–(l) showed that NO_x emissions increased drastically with increasing engine load. At higher engine loads, combustion chamber temperatures increased due to combustion of relatively higher fuel quantity. NO_x emissions also showed a close relationship with combustion phasing because peak combustion chamber temperature increased with advanced combustion phasing due to relatively earlier ignition and higher T_i, leading to higher NO_x emissions. NO_x emissions were almost similar for all test fuels, with mineral diesel emitting slightly lower NO_x emissions (Figure 10(j)–(l)). Improved fuel vaporization of diesohol, diesoline and diesosene led to advanced combustion phasing. B20 showed slightly higher NO_x emissions compared to mineral diesel (Figure 10(j)). This was because of poor vaporization of this test fuel resulting in formation of heterogeneous fuel–air mixtures, which shifted combustion towards diffusion combustion phase. This led to higher in-cylinder temperatures. Presence of fuel-bound oxygen also favored NO_x formation in case of B20. All test fuels showed higher NO_x emissions at higher T_i. This was because of faster fuel–air mixture chemical kinetics, which resulted in advanced combustion phasing. Effect of higher T_i was dominant at higher engine loads, but at lower loads, effect of T_i was negligible (Figure 10(j)–(l)).

Although PAHs are unregulated pollutants, they have severe human health impact. PAHs were emitted in vapor form and were also adsorbed onto particulate surface. Figure 10(m)–(o) showed that total PAH emissions increased with increasing engine load (i.e. richer fuel–air mixtures). At all engine loads and T_is, mineral diesel and diesoline showed the lowest PAH emissions, while diesosene displayed the highest emissions. Combustion kinetics of fuel–air mixture was the main factor, which affected PAH formation during PHCCI combustion mode. Emissions of PAHs depends on engine load and test fuel properties. PAH emissions slightly increased with increasing T_is. For most engine operating conditions, total PAH emissions were in the range of 200–1200 ng/m^3; however, for very rich fuel–air mixture engine operating conditions, PAH emissions were in the range of 1000–1250 ng/m^3.

Particulate characteristics

This section shows the particulate characteristics of the PHCCI engine at different engine loads and T_is. Particulate characteristics were measured using EEPS. At each experimental condition, particulates were sampled for 1 min at a sampling frequency of 1 Hz. Average of these 60 data points is presented in this section. Particulate characteristics mainly include four parameters, namely, number-size distribution, surface area-size distribution, mass size distribution and statistical analysis of particulates.

Figure 11(a)–(r) showed the number-size distribution of particulates emitted from the PHCCI engine at different operating conditions. Particle number-size distribution shows the number concentration of particulates of specific size range. Based on size, particulates can be divided into three regimes, namely, nano-particles (NP) ($D_p < 10$ nm), NMP ($D_p < 50$ nm) and AMP (50 nm $< D_p <$ 1000 nm).

Among all test fuels, B20 exhibited the highest particulate concentration, while diesohol showed the lowest particulate concentration. Relatively higher viscosity and lower volatility of biodiesel was the main factor for this behavior, which resulted in slightly inferior fuel vaporization and fuel–air mixture inhomogeneity in the combustion chamber. Due to presence of fuel-rich zones, PHCCI combustion mode resulted in higher soot nuclei formation. Effect of volatile additives can be clearly seen from the particulate characteristics. At most engine operating conditions (especially at higher loads), diesoline, diesohol and diesosene resulted in slightly lower particulate concentration compared to baseline mineral diesel. Due to improved volatility, these test fuels resulted in more homogeneous fuel–air mixture formation, therefore lower soot nuclei formation. Among diesoline, diesohol and diesosene, diesosene showed slightly higher particulate concentration in AMP regime. This was due to presence of soluble impurities in kerosene, which acted as soot precursors leading to formation of higher number of particulates. Combined effect of higher volatility and presence of fuel-bound oxygen in diesohol was the main reason for the lowest particulate concentration. Presence of fuel-bound oxygen in diesohol improved fuel oxidation and resulted in lower soot nuclei formation. Amongst all test fuels, B20 showed the highest number concentration of NPs ($\sim 10^6$ particles/cm^3 of exhaust gas). At higher engine loads, relatively more volatile test fuels resulted in slightly lower number concentration of NPs compared to mineral diesel.

Results also showed that concentration of particulates increased with increasing engine load (Figure 11(a), (d), (g), (j), (m) and (p)). This trend was common for all test fuels and was mainly due to presence of relatively richer fuel–air mixtures at higher engine loads, which resulted in formation of higher number of soot nuclei. Most particulate emitted by the PHCCI engine were in the size range of ~70–120 nm. At higher engine loads, peaks of particulate number-size distribution shifted towards bigger particle sizes. This showed that the tendency of particulate agglomeration and coagulation was higher at higher engine loads. This was mainly due to formation of significantly higher PAHs, which were adsorbed on the particulate surfaces, leading to larger particulates (Figure 10(m)–(o)). At all engine loads, presence of NPs can be clearly seen in particulate number-size distributions. Concentration of NPs slightly decreased with decreasing engine load. This happens mainly due to two factors, namely, lower HRR and longer CD. Relatively lower fuel injection

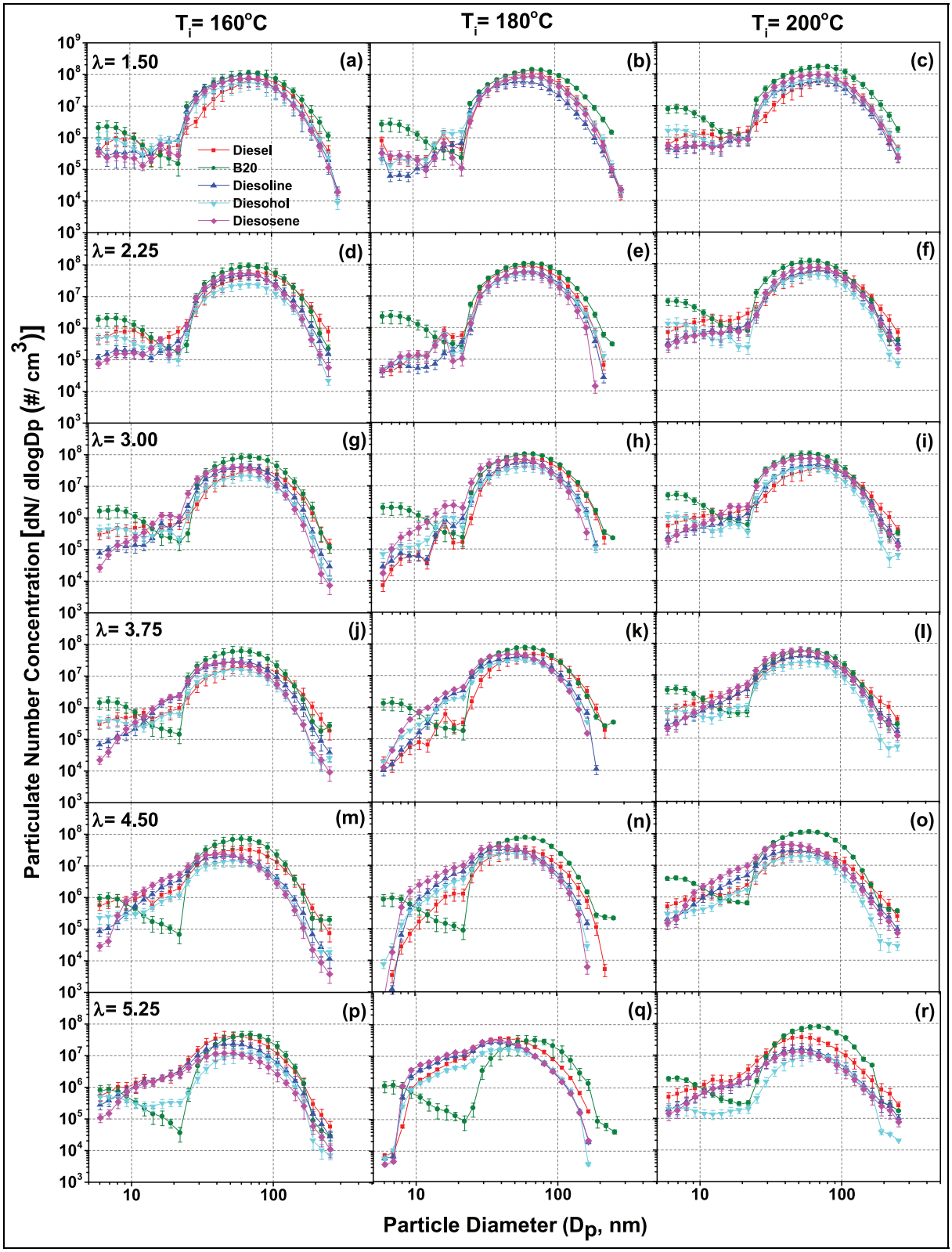

Figure 11. (a–r) Number-size distribution of particulates emitted from PHCCI engine fueled by mineral diesel, B20, diesoline, diesohol and diesosene at different engine loads and T_is.

quantity and dominant effect of EGR at lower engine loads were responsible for lower HRR, which reduced the nuclei formation and longer CD promoted soot agglomeration and coagulation processes. Combined effect of these two factors resulted in lower number concentration of NPs at lower engine loads. Difference between particulate concentration of different test fuels in AMP regime increased with decreasing engine load;

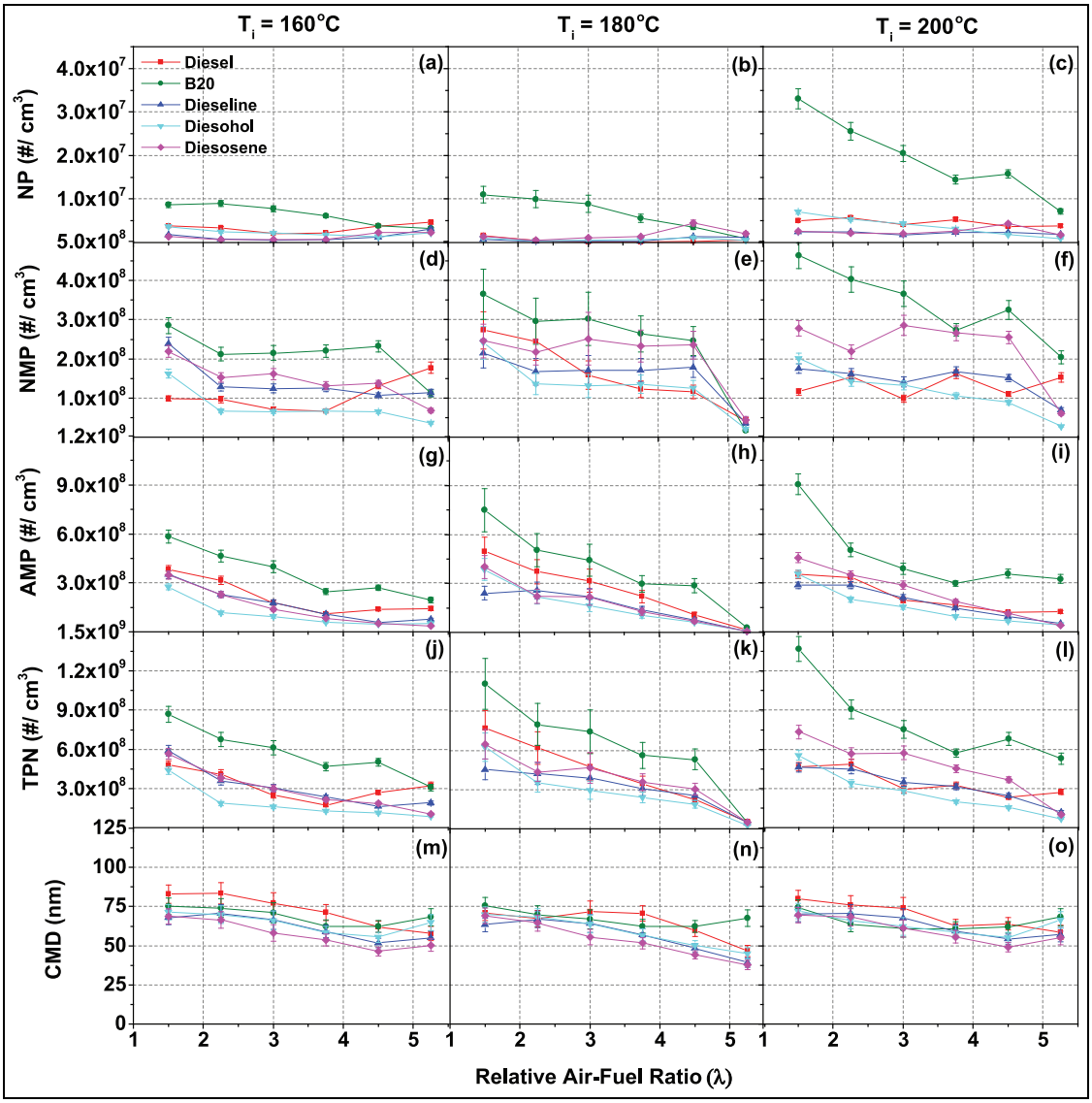

Figure 12. (a-c) NP, (d-f) NMP, (g-i) AMP and (j-l) TPN concentration and (m-o) CMD of particulates emitted by PHCCI engine fueled by mineral diesel, B20, diesoline, diesohol and diesosene at different engine loads and T_is.

however, difference in number concentration of NPs decreased.

At higher engine loads, increasing T_i resulted in slightly higher particulate number concentration; however, peak of particulate number-size distribution shifted toward smaller particle sizes (Figure 11(b), (e), (h) and (k)). At higher T_i, combustion efficiency improved slightly, which led to formation of slightly higher number of particulates due to presence of richer fuel–air mixture. At T_i = 200 °C, particulate emissions in NMP and AMP regimes reduced slightly; however, emission of NPs increased. This was attributed to contribution of lubricating oil to the formation of particulates. At higher T_i, incomplete combustion of lubricating oil resulted in soot nuclei formation leading to higher NPs formation.[52] At lower engine loads, particulate emissions slightly reduced with increasing T_i (Figure 11(n), (o), (q) and (r)). This was because of presence of leaner fuel–air mixture, which led to lesser particulate formation. At lower engine loads, wider particulate number-size distributions showed significant increase in emissions of smaller particulates. Effect of increasing T_i on particulate emissions was also dependent on fuel volatility. At all engine loads, particulate emissions from B20 increased with increasing T_i. However, particulate emissions from mineral diesel, diesoline, diesohol and diesosene increased up to T_i = 180 °C and further increase in T_i (up to 200 °C) resulted in slightly lower particulate emissions.

Figure 12 shows the variation of NPs (Figure 12(a)–(c)), NMPs (Figure 12(d)–(f)), AMPs (Figure 12(g)–(i)), total particulate number (TPN) concentration (Figure 12(j)–(l)), and count mean diameter (CMD) of particulates (Figure 12(m)–(o)) at different

engine loads and T_is. These parameters were calculated mathematically from the number-size distribution of particulates emitted in PHCCI combustion mode.

Figure 12(a)–(c) shows the variations in concentration of NPs emitted from PHCCI combustion of different test fuels. Carbon nano-tubes and fibers emissions have been reported by many researchers as byproducts of diesel combustion.[53] There is already a focus of toxicological studies. The results obtained so far have showed that B20 emitted significantly higher concentration of NPs compared to other test fuels. This was attributed to higher number of soot nuclei formation. Concentration of NPs from B20 reduced with decreasing engine load, though other test fuels showed almost constant number concentrations ($\sim 10^7$ particles/cm^3 of exhaust gas) at different engine loads. Further concentration of NPs from B20 increased with increasing T_i, while other test fuels showed lowest number concentration at $T_i = 180\,^{\circ}C$. Figure 12(d)–(f) showed the variation of NMP concentrations emitted from PHCCI combustion using different test fuels. Concentration of NMP were affected by several parameters such as engine load, fuel properties and T_i. These parameters control the chemical kinetics of fuel–air mixtures, which directly affect combustion. Due to lower in-cylinder temperatures in the PHCCI engine, presence of higher concentrations of unburned HCs and PAHs promoted soot nucleation and resulted in higher NMP concentration. Results showed that concentration of NMP varied from 5×10^7 to 5×10^8 particles/cm^3 of the exhaust gas, which slightly decreased with decreasing engine loads. This was mainly due to presence of leaner fuel–air mixtures, which led to lower nuclei formation. At lower engine loads, longer CD promoted coagulation of NMPs which resulted in slightly lower number concentration of NMPs. Among all test fuels, B20 showed the highest concentration of NMPs followed by diesosene and diesohol (lowest number concentration). With increasing T_i, concentration of NMPs from B20, diesosene and diesohol increased. However, NMPs concentration of mineral diesel and diesoline first increased (up to 180 °C) and then decreased slightly (up to 200 °C). Figure 12(g)–(i) showed the variations in of AMP number concentration emitted by PHCCI engine using different test fuels. Number concentration of AMPs varied from 1×10^8 to 9×10^8 particles/cm^3 of the exhaust gas. For all test fuels, number concentration of AMPs decreased at lower engine loads. This was mainly due to formation of lesser amount of PAHs at lower engine loads, which were adsorbed on the primary particulates and resulted in formation of AMPs. Among all test fuels, B20 resulted in highest AMP number concentration, and diesohol showed the lowest number concentration. AMP number concentration slightly increased with increasing T_i (up to 180 °C); however, with further increase in T_i (up to 200 °C), there was insignificant difference in number concentration. Figure 12(j)–(l) showed the variation of TPN emitted from PHCCI engine using different test fuels. Results showed that TPNs decreased with increasing λ. This was attributed to reduction in concentration of both NMPs and AMPs at lower engine loads. Among all test fuels, B20 showed highest TPNs, and diesohol showed the lowest TPNs. In general, TPNs slightly increased with increasing T_i; however, at $T_i = 200\,^{\circ}C$, mineral diesel and diesoline showed relatively lower TPNs compared to that at $T_i = 180\,^{\circ}C$. Effect of volatile additives can be clearly observed from the trends of TPNs. Addition of volatile additives resulted in lower TPNs compared to mineral diesel. At $T_i = 200\,^{\circ}C$, diesosene showed slightly higher TPNs compared to mineral diesel. This was mainly due to higher concentration of NMPs, which were produced due to impurities in kerosene, and availability of PAHs promoted their growth up to nucleation size range. Figure 12(m)–(o) showed the variation of CMD of particulates emitted from PHCCI engine fueled by different test fuels. CMD is a measure of average particulates size. Higher or lower CMD of particulates shows the dominance of bigger or smaller particulates, respectively. Results showed that CMD of particulate slightly decreased with decreasing engine load. This was mainly due to reduction in PAHs, which directly influenced particulates growth via agglomeration and coagulation. Among all test fuels, mineral diesel showed the highest CMD, and diesosene showed the lowest CMD. This was mainly because of the dominance of bigger particles ($D_p > 100$ nm) in mineral diesel exhaust. Relatively lower TPNs and higher fraction of NMPs were the main reasons for lowest CMD of particulate emitted by mineral diesel. For all test fuels, increasing T_i (up to 180 °C) resulted in slight reduction in CMD of particulate; however, further increase in T_i resulted in slightly higher CMD of particulate. This was mainly due to dominance of AMPs at higher T_i.

Figure 13 shows the surface area-size distributions of particulates emitted from the PHCCI engine by different test fuels. Surface area-size distribution is an important characteristic of particulates emitted from engine because it is a direct measure of toxicity. Higher surface area provides more active sites for adsorption of toxic volatile species and PAHs onto primary particulates. Higher surface area corresponding to relatively smaller particulates increases the human health risk potential because of two combined effects. Smaller particulates can penetrate deeper into human respiratory system, and larger quantities of toxic species adsorbed on their surface gets dissolved in blood, leading to harmful diseases. Shape and size of particulates depend on several parameters such as engine operating condition, engine load, dilution condition and the engine design. However, in present investigations, particulate surface area was calculated by assuming them to be spherical[54]

$$dS = dN.\left(D_p\right)^2$$

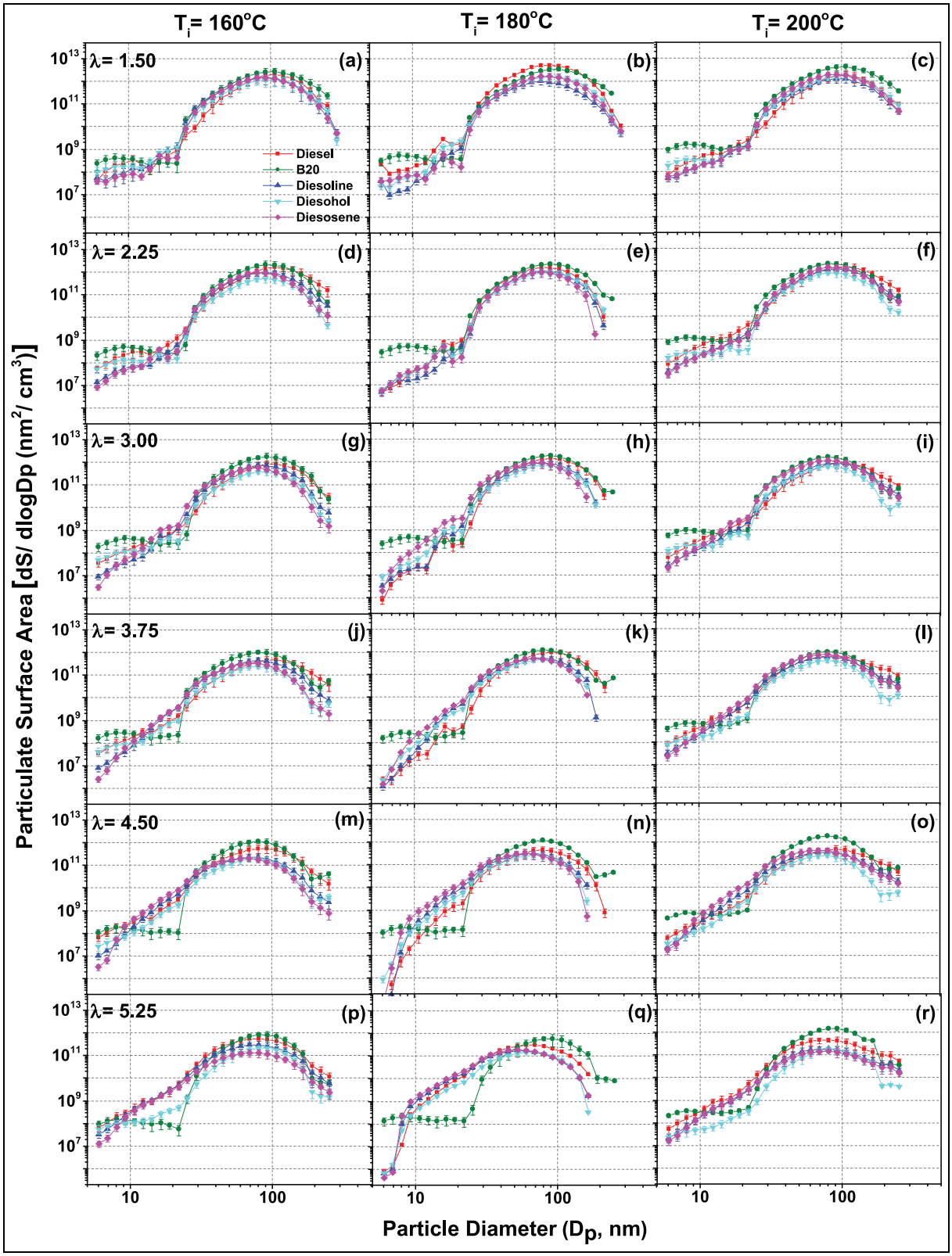

Figure 13. (a-r) Surface area-size distribution of particulates emitted from PHCCI engine fueled by mineral diesel, B20, diesoline, diesohol and diesosene at different engine loads and T_is.

Here, dS is the surface area of particles in the size range with mean diameter D_p, and dN being the number concentration of particulates with mean diameter D_p. From the results obtained, it was observed that peaks of particulate surface area size distribution lie in AMP regime. This indicated larger contribution of bigger particles to particulate surface area distribution.

For all test fuels, particulate surface area increased with increasing engine load. Presence of relatively higher fuel quantity at higher load was the main reason

for this trend. At higher engine loads, PAHs formed get adsorbed on to the particulate surface, leading to higher particulate surface area. Contribution of NPs to particulate surface area distribution was an important finding of this study. Among all test fuels, B20-fueled PHCCI combustion mode resulted in significantly higher particulate surface area in NP regime, which slightly decreased with decreasing engine load. Addition of volatile additives in mineral diesel resulted in lower particulate surface area. Among all test fuels, B20 showed the highest particulate surface areas in both NP and AMP regimes; however, diesosene resulted in the highest particulate surface area in NMP regime. This showed dominance of NMP number concentration in diesosene-fueled PHCCI engine exhaust. Diesohol showed the minimum particulate surface area distribution due to lower number concentration of particulates. At higher engine loads, increasing T_i resulted in slightly higher particulate surface area distribution, though at lower engine loads, the surface area distribution showed no significant difference at different T_is. Particulate surface area corresponding to NP regime increased with increasing T_i. This was mainly because of increase in number concentration of NPs. Among all test fuels, B20 was found to be the most sensitive to T_i variations.

Figure 14 shows the particulate mass-size distribution of particulates emitted by the PHCCI engine for different test fuels. Particulate mass-size distributions showed the relative dominance of particulate mass in different size ranges. Particulate mass was calculated from the particulate number-size distributions of particulates by assuming them to be spherical and of constant density. For particulates mass distribution calculations, density of a particulates was assumed to be 1 g/cm^3.[54] Lighter particulates are more harmful for human health compared to heavier particulates. Particulates with higher mass settle down faster on to the ground thereby reducing their probability to be inhaled by the human respiratory system. However, lighter particles have longer retention time in the atmosphere, which increases their probability to be inhaled. Due to their smaller size, lighter particulates also penetrate deeper into the respiratory system, which is quite harmful for the human health.

Figure 14 shows that particulate mass distribution corresponding to bigger particulates was significantly higher compared to relatively smaller particulates. For all test fuels, NPs showed significantly lower particulate mass compared to NMPs and AMPs. Furthermore, particulate mass decreased with decreasing engine load. This was mainly due to presence of relatively lower fuel quantity injected at lower engine loads.

With increasing engine load, particulate mass-size distributions shifted toward smaller size particulates. Among all test fuels, B20 showed the highest particulate mass followed by mineral diesel. Effect of volatile additives was also clearly evident from the particulate mass-size distribution. Contrary to particulate number-size and surface area-size distributions, particulate mass-size distribution of diesosene was slightly lower compared to other test fuels. This showed relatively lesser contribution of kerosene to particulate mass corresponding to NP and AMP regimes. At higher engine loads, particulate mass increased with increasing T_i, but at lower engine loads, particulate mass first increased (up to 180 °C) and then decreased with further increase in T_i. This was mainly because of the relative dominance of particulate number-size distributions.

Trace metal analysis

Figure 15(a)–(d) shows variations in particulate bound trace metals at $\lambda = 3.0$, $T_i = 180$ °C and 10% EGR. The trace metals emitted in exhaust particulates were determined by inductively coupled plasma optical emission spectrophotometer (ICP-OES). Some of the trace metals detected were below the detectable limit of the instrument. Only those elements, which were detected with 90% confidence level, are reported here. Trace metal concentrations were evaluated in mg/g of the particulate mass for relative comparison. Experiments were carried out only at medium engine load ($\lambda = 3$) to investigate comparative trace metal emission characteristics of different test fuels in PHCCI mode. Particulates contain trace metals such as Zn, Fe, Cr, Cd, As, Sr, Pb, Mg, Na, K, Ni and Al. Some of the trace metals such as Cr and Ni are considered as probable carcinogens. Trace metals also act as nuclei for the adsorption of organic compounds, leading to particulate formation. There are three main sources of trace metals in engine exhaust, which includes fuel-borne trace metals, residues of wear debris from moving parts and additives from lubricating oil. Fuel contains traces of elements like Ca, K, Na and Mg, while Zn, Cu and Al mainly originate from the lubricating oil. In this analysis, all trace metals are suggested in four different categories based on their source, health effects and concentrations.

Figure 15 shows that addition of volatile additives resulted in negligible difference in several trace metals concentrations such as As, Sr, Mg, K and Cu; however, some of the trace metals such as Fe, Na, Zn, Mn and Ni showed high sensitivity to different test fuels. Among all trace metals, As was detected in minimum concentration (Figure 15(a)) and Na was detected in highest concentration (Figure 15(c)). Diesohol showed relatively higher trace metal concentrations compared to diesoline and diesosene. Among all test fuels, B20 showed slightly lower trace metal concentration. This was attributed to lower particulate mass (Figure 14). In absolute units, diesohol and diesoline resulted in lowest concentrations of most trace metals (Figure 15(a)–(d)). This observation can be explained by the improved

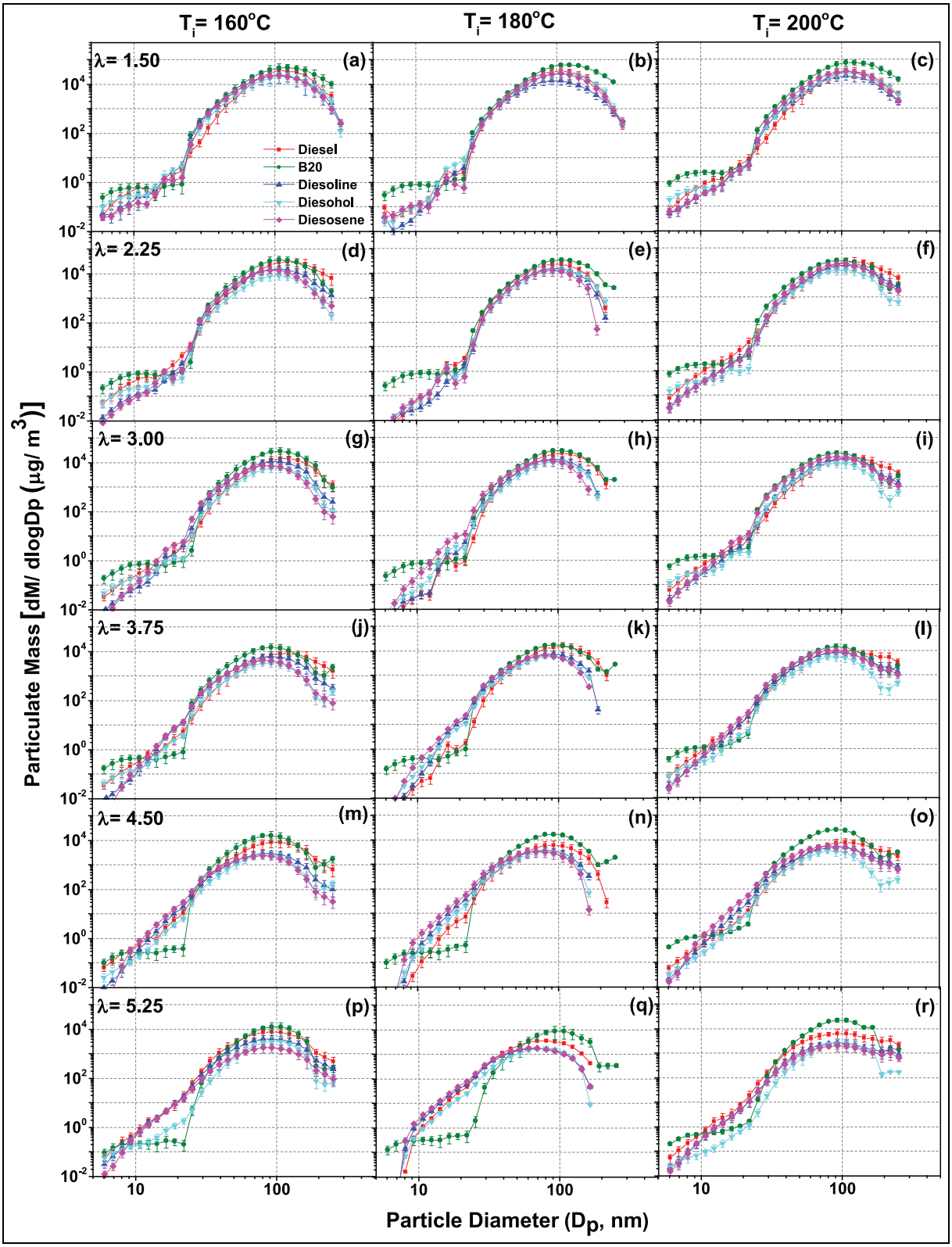

Figure 14. (a-r) Mass-size distributions of particulates emitted from the PHCCI engine fueled by mineral diesel, B20, diesoline, diesohol and diesosene at different engine loads and T_is.

thermal efficiency, which reduced ISEC. This was reflected in reduced emissions of trace metals.

For most trace metals, such as Al, Na and Mn, diesosene and mineral diesel showed the maximum concentration in particulates. This was mainly due to relatively higher in-cylinder pressure and temperature, which resulted in intense in-cylinder conditions. Under such intense in-cylinder conditions, tendency of

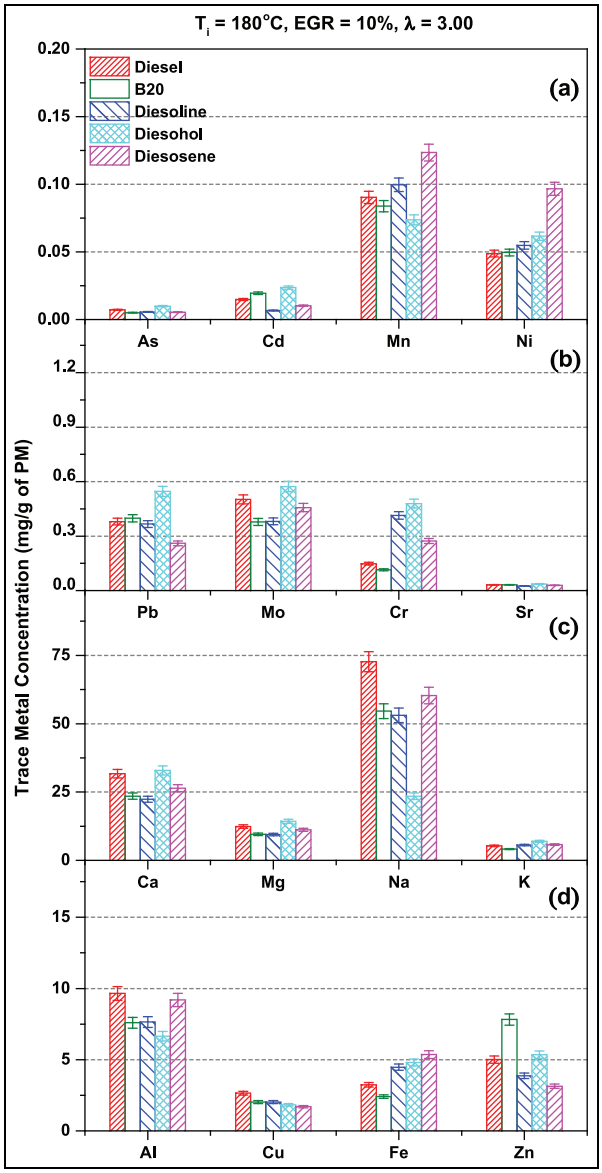

Figure 15. (a-d) Particulate-bound trace metals emitted by PHCCI engine fueled with mineral diesel, B20, diesoline, diesohol and diesosene.

lubricating oil decomposition and engine wear increased, which resulted in higher trace metal concentrations in the particulates.

As and Cd were found in very small concentrations in the particulates, and different test fuels did not show any significant difference (Figure 15(a)). Mn was present in particulates due to pyrolysis of lubrication oil at higher in-cylinder temperatures. Concentration of Mn varied from 0.1 to 0.15 mg/g of particulates. Mn was slightly higher for mineral diesel, diesoline and diesosene (Figure 15(a)). Ni is used as an additive in the lubricating oil in very small concentration as Nickel ethoxy-ethylxanthate, which improves its lubrication quality. Upon combustion, these compounds dissociate to release Ni, which emerges in the exhaust particulates and may cause various harmful health issues. Diesosene particulates showed maximum Ni concentration due to higher in-cylinder pressure and temperature (Figures 5 and 9), which promoted the pyrolysis of lubricating oil.

Pb, Mo and Cr were also found in PHCCI particulates (Figure 15(b)). Main source of these trace metals were fuel and lubricating oil. Trace concentration of these metals varied from 0.2 to 0.6 mg/g of particulates. Diesohol showed the highest concentration of these metals due to lower particulate mass; however, mineral diesel and diesosene resulted in maximum concentration of Pb and Mo (Figure 15(b)). Ca, Na, K and Mg entered the exhaust gas from the fuel and lubricating oil (Figure 15(c)). However, these trace metals could be ignored due to their lower adverse impact on human health. Fe, Cu, Al and Zn enter the exhaust particulates from engine wear and the lubricating oil. These trace metals are very harmful to the human health because they have significant reactive oxygen species (ROS) generation potential. Al trace concentration was found to be in the range of 8–10 mg/g of particulates (Figure 15(d)). Al originates mainly from the engine wear. Friction due to relative movement between mating parts causes slightly higher Al traces compared to other trace metals in this category. Among all test fuels, mineral diesel and diesosene resulted in slightly higher Al trace emission compared to other test fuels. Intense in-cylinder conditions might be a possible reason for this behavior. Fe concentration was found to be in the range of 0–6 mg/g of particulates. Diesosene showed the maximum Fe concentration followed by diesohol and diesoline. Presence of metallic impurities resulted in higher Fe in diesosene PHCCI combustion. Copper originated from the lubricating oil as well as wear of engine components. For all test fuels, Cu concentration varied from 2 to 3 mg/g of particulates (Figure 15(d)). Zinc-containing additives such as zinc dialkyl dithiophosphate (ZDDP) is a commonly used additive in the lubricating oils and greases. When the lubricating oil heats above 100 °C, ZDDP decomposes in presence of oxygen and forms zinc polyphosphate. Zinc polyphosphate reacts with iron oxide in the combustion chamber to produce ZnO. In high-temperature environment, ZnO redox reaction occurs to form Zinc, which is emitted as trace metal in the particulates. Due to presence of oxygen in the fuel, B20 and diesohol resulted in slightly higher Zn traces in the particulates compared to other test fuels.

Conclusions

In this study, effects of T_i and fuel volatility on PHCCI engine combustion, performance, emissions and particulate characteristics were experimentally investigated using different test fuels, namely, B20, diesoline, diesohol, diesosene vis-à-vis baseline mineral diesel. Experiments were performed at three different T_is (160, 180 and 200 °C) and six engine loads. These experimental investigations showed significant effect of volatile additives on combustion phasing, which is an

important parameter for PHCCI combustion. Diesoline and diesohol showed improved combustion phasing though diesosene resulted in advanced combustion phasing. Due to inferior volatility and lower calorific value of biodiesel, B20 displayed retarded combustion phasing. At lower engine loads, addition of volatile additives improved SoC and HRR; however, excessive knocking was observed at higher engine loads. Diesoline and diesosene showed significant improvement in ITE and ISFC for B20 yielding relatively higher ISFC. PHCCI combustion of diesoline, diesohol and diesosene resulted in lower HC and CO emissions compared to mineral diesel. PAHs analysis showed slightly lower concentration of PAHs from diesoline; however, other test fuels resulted in slightly higher concentrations of PAHs compared to baseline mineral diesel. Addition of volatile additives resulted in lower particulate emissions; however, B20-fueled PHCCI combustion showed significantly higher number concentrations of NPs compared to other test fuels. Presence of significant number concentration of NPs in PHCCI engine exhaust was another important finding of this study. Increasing T_i affected fuel–air mixing which resulted in slightly lower CO and HC emissions at 180 °C. Increasing T_i improved combustion stability at low engine loads; however, higher T_i led to unstable combustion (excessive knocking at 200 °C) at intermediate loads. At higher engine loads, particulate emissions increased slightly with increasing T_i. Particulate mass corresponding to NP regime increased with increasing T_i. Particulate composition analysis showed that mineral diesel- and diesosene-fueled PHCCI engine emitted the maximum concentration of most trace metals in the particulates.

Overall, this study demonstrated that mineral diesel–fueled PHCCI combustion can be improved by addition of volatile additives such as gasoline, alcohols and kerosene. This study showed significant potential of low-quality, low-cetane fuels as additives, which improve the combustion and performance characteristics of PHCCI engine. Problems associated with use of a fuel vaporizer at higher engine loads can be significantly reduced by increasing T_i, which ultimately expands the operating window of PHCCI combustion.

Declaration of conflicting interests

The author(s) declared no potential conflicts of interest with respect to the research, authorship and/or publication of this article.

Funding

The author(s) disclosed receipt of the following financial support for the research, authorship, and/or publication of this article: The authors are grateful to Technology Systems Group, Department of Science and Technology (DST), Government of India for providing financial support (Grant no. DST/TSG/AF/2011/144-G dated 14-01-2013) for carrying out this study. Financial support from Council for Scientific and Industrial Research (CSIR), Government of India's Senior Research Associate (SRA) scheme to Dr A.P.Singh is highly acknowledged, which supported his stay at ERL, IIT Kanpur for conducting these exhaustive series of experiments.

References

1. Akihama K, Takatori Y, Inagaki K, Sasaki S and Dean AM. Mechanism of the smokeless rich diesel combustion by reducing temperature. SAE technical paper 2001-01-0655, 2001.
2. Onishi S, Jo SH, Shoda K, Do Jo P and Kato S. Active thermo-atmosphere combustion (ATAC)—a new combustion process for internal combustion engines. SAE technical paper 790501, 1979.
3. Najt PM and Foster DE. Compression-ignited homogeneous charge combustion. SAE technical paper 830264, 1983.
4. Ryan TW and Callahan TJ. Homogeneous charge compression ignition of diesel fuel. SAE technical paper 961160, 1996.
5. Laguitton O, Crua C, Cowell T, Heikal MR and Gold MR. The effect of compression ratio on exhaust emissions from a PCCI diesel engine. *Energ Convers Manage* 2007; 48(11): 2918–2924.
6. Araki M, Umino T, Obokata T, Ishima T, Shiga S and Nakamura H. Effects of compression ratio on characteristics of PCCI diesel combustion with a hollow cone spray. SAE technical paper 2005-01-2130, 2005.
7. Horibe N, Harada S, Ishiyama T and Shioji M. Improvement of premixed charge compression ignition-based combustion by two-stage injection. *Int J Engine Res* 2009; 10(2): 71–80.
8. Agarwal AK, Singh AP and Maurya RK. Evolution, challenges and path forward for low temperature combustion engines. *Prog Energ Combust* 2017; 61: 1–56.
9. Torregrosa AJ, Broatch A, García A and Mónico LF. Sensitivity of combustion noise and NO_x and soot emissions to pilot injection in PCCI Diesel engines. *Appl Energ* 2013; 104: 149–157.
10. Boot M, Luijten C, Rijk E, Albrecht B and Baert RSG. Optimization of operating conditions in the early direct injection premixed charge compression ignition regime. SAE technical paper 2009-24-0048, 2009.
11. Kalghatgi GT, Risberg P and Ångstom HE. Partially premixed auto-ignition of gasoline to attain low smoke and low NO_x at high load in a compression ignition engine and comparison with a diesel fuel. SAE technical paper 2007-01-0006, 2007.
12. Kalghatgi GT. Auto-ignition quality of practical fuels and implications for fuel requirements of future SI and HCCI engines. SAE technical paper 2005-01-0239, 2005.
13. Xu HM, Misztal J, Wyszynski ML, Turner D, Price P, Stone R, et al. HCCI—how clean can it be? In: *Proceedings of the homogeneous charge compression ignition (HCCI) symposium*, Lund, Sweden, 12–14 September 2007.

14. Chao Y, Jian-xin W, Zhi W and Shi-jin S. Comparative study on Gasoline Homogeneous Charge Induced Ignition (HCII) by diesel and Gasoline/Diesel Blend Fuels (GDBF) combustion. *Fuel* 2013; 106: 470–477.
15. Han D, Ickes AM, Bohac SV, Huang Z and Assanis DN. Premixed low-temperature combustion of blends of diesel and gasoline in a high speed compression ignition engine. *P Combust Inst* 2011; 33: 3039–3046.
16. Turner D, Tian G, Xu H, Wyszynski M and Theodoridis E. An experimental study of diesoline combustion in a direct injection engine. SAE technical paper 2009-01-1101, 2009.
17. Zhang RD, He H, Shi XY, Zhang CB, He BQ and Wang JX. Preparation and emission characteristics of ethanol-diesel fuel blends. *J Environ Sci* 2004; 16(5): 793–799.
18. Ahmed I. Oxygenated diesel: emissions and performance characteristics of ethanol-diesel blends in CI engines. SAE technical paper 2001-01-2475, 2001.
19. He BQ, Shuai SJ, Wang JX and He H. The effect of ethanol blended diesel fuels on emissions from a diesel engine. *Atmos Environ* 2013; 37: 4965–4971.
20. Saxena S, Schneider S, Aceves S and Dibble R. Wet ethanol in HCCI engines with exhaust heat recovery to improve the energy balance of ethanol fuels. *Appl Energ* 2012; 98: 448–457.
21. Saxena S, Vuilleumier D, Kozarac D, Krieck M, Dibble R and Aceves S. Optimal operating conditions for wet ethanol in a HCCI engine using exhaust gas heat recovery. *Appl Energ* 2014; 116: 269–277.
22. Macka JH, Aceves SM and Dibble RW. Demonstrating direct use of wet ethanol in a homogeneous charge compression ignition (HCCI) engine. *Energy* 2009; 34(6): 782–787.
23. Ishida M, Yamamoto S, Ueki H and Sakaguchi D. Remarkable improvement of NO_x–PM trade-off in a diesel engine by means of bioethanol and EGR. *Energy* 2010; 35: 4572–4581.
24. Fang T, Lin YC, Tien MF and Lee CF. Reducing NO_x emissions from a biodiesel-fueled engine by use of low-temperature combustion. *Environ Sci Technol* 2008; 42: 8865–8870.
25. Verma G, Sharma H, Thipse SS and Agarwal. Spark assisted premixed charge compression ignition engine prototype development. *Fuel Process Technol* 2016; 152: 413–420.
26. Teoh YH, Masjuki HH, Kalam MA, Amalina MA and How HG. Impact of premixed kerosene fuel on performance, emission and combustion characteristics in partial HCCI engine. *Enrgy Proced* 2014; 61: 1830–1834.
27. Singh AP and Agarwal AK. Diesoline, diesohol, and diesosene fuelled HCCI engine development. *J Energ Resour: ASME* 2015; 138(5): 052212.
28. Yadav S, Murthy K, Mishra D and Baral B. Estimation of petrol and diesel adulteration with kerosene and assessment of usefulness of selected automobile fuel quality test parameters. *Int J Environ Sci Te* 2005; 1(4): 253–258.
29. Pathak S, Aigal AK, Sharma ML, Narayanan L and Saxena M. Reduction of exhaust emissions in a kerosene operated genset for electrical energy applications. SAE technical paper 2005-26-026, 2005.
30. Bergstrand P. Effects on combustion by using kerosene or MK1 diesel. SAE technical paper 2007-01-0002, 2007.
31. Singh G, Singh AP and Agarwal AK. Experimental investigations of combustion, performance and emission characterization of biodiesel fuelled HCCI engine using external mixture formation technique. *Sustain Energ Technol Assessm* 2014; 6: 116–128.
32. Singh AP and Agarwal AK. Combustion characteristics of diesel HCCI engine: an experimental investigation using external mixture formation technique. *Appl Energ* 2012; 99: 116–125.
33. Midlam-Mohler S. Diesel HCCI with external mixture preparation. In: *Proceedings of 10th diesel engine emissions reduction (DEER) workshop*, Newport, USA, 29 August–2 September 2004.
34. Ganesh D and Nagarajan G. Homogeneous charge compression ignition (HCCI) combustion of diesel fuel with external mixture formation. SAE technical paper 2009-01-0924, 2009.
35. Midlam-Mohler S, Guezennec Y and Rizzoni G. Mixed-mode diesel HCCI with external mixture formation. In: *Proceedings of the 9th diesel engine emissions reduction (DEER) workshop*, USA, 2003.
36. Canova M, Midlam-Mohler S, Guezennec Y and Rizzoni G. Mean value modeling and analysis of HCCI diesel engines with external mixture formation. *J Dyn Syst: T ASME* 2009; 131: 011002.
37. Puschmann H, Buchwald R, Pannwitz M, Sommer A, vom Schloß HP and Lucka K. Homogeneous diesel combustion with external mixture formation by a cool flame vaporizer. SAE technical paper 2006-01-3323, 2006.
38. Singh AP and Agarwal AK. Effect of intake charge temperature and EGR on biodiesel fuelled HCCI engine. SAE technical paper 2016-28-0257, 2016.
39. Zhang C-H, Pan J-r, Tong J-j and Li J. Effects of intake temperature and excessive air coefficient on combustion characteristics and emissions of HCCI combustion. *Procedia Environ Sci* 2011; 11: 1119–1127.
40. Gowthaman S and Sathiyagnanam AP. Effects of charge temperature and fuel injection pressure on HCCI engine. *Alexandria Eng J* 2016; 55: 119–125.
41. Ramesh A, Swami Nathan S and Mallikarjuna JM. An experimental study of the biogas–diesel HCCI mode of engine operation. *Energ Convers Manage* 2010; 51: 347–1353.
42. Li G, Zhang CH, Shen YC, Shen YC and Zhou JW. Effects of intake temperature on the combustion characteristics of HCCI engine fueled with n-butanol. *Appl Mech Mater* 2015; 98: 651–654.
43. Persson H, Agrell M, Olsson J, Johansson B and Ström H. The effect of intake temperature on HCCI operation using negative valve overlap. SAE technical paper 2004-01-0944, 2004.
44. Asad U, Zheng M, Ting DS-K and Tjong J. Implementation challenges and solutions for homogeneous charge compression ignition combustion in diesel engines. *J Eng Gas Turb Power* 2015; 137: 101505.
45. Franklin L. *Effects of homogeneous charge compression ignition (HCCI) control strategies on particulate emissions of ethanol fuel*. Minneapolis, MN: University of Minnesota, 2010.
46. Agarwal AK, Lukose J, Singh AP and Gupta T. Characterization of exhaust particulates from diesel fueled homogenous charge compression ignition combustion engine. *J Aerosol Sci* 2013; 58: 71–85.
47. Agarwal AK, Gupta T, Lukose J and Singh AP. Particulate characterization and size distribution in the exhaust

of a gasoline homogeneous charge compression ignition engine. *Aerosol Air Qual Res* 2014; 15(2): 504–516.
48. Borm PJA, Robbins D, Haubold S, Kuhlbusch T, Fissan H, Donaldson K, et al. The potential risks of nanomaterials: a review carried out for ECETOC. *Part Fibre Toxicol* 2006; 3: 11.
49. Kittelson DB. Recent measurements of nanoparticle emissions from engines. In: *Proceedings of the meeting on current research on diesel exhaust particles*, Japan Association of Aerosol Science and Technology, Kyoto, Japan, 9 January 2001.
50. Fialkov AB. Investigations on ions in flames. *Prog Energ Combust* 1997; 23: 399–528.
51. *User manual of AVL indo-micro software*. *Exploration guide: AVL INDICOM 2014*. Graz: AVL List GmbH, 2014.
52. Singh AP, Pal A and Agarwal AK. Comparative particulate characteristics of hydrogen, CNG, HCNG, gasoline and diesel fueled engines. *Fuel* 2016; 185: 491–499.
53. Evelyn A, Mannick S and Sermon PA. Unusual carbon-based nanofibers and chains among diesel-emitted particles. *Nano Lett* 2003; 3: 63–64.
54. *Engine exhaust particle sizer™ spectrometer model 3090* (Operation and service manual, March). Shoreview, MN: TSI, 2009.